USGS
science for a changing world

Prepared in cooperation with the U.S. Geological Survey Water Availability and Use Science Program

Documentation for the "XT3D" Option in the Node Property Flow (NPF) Package of MODFLOW 6

Chapter 56 of
Section A, Groundwater
Book 6, Modeling Techniques

Techniques and Methods 6–A56

U.S. Department of the Interior
U.S. Geological Survey

Cover. Binary computer code illustration.

Documentation for the "XT3D" Option in the Node Property Flow (NPF) Package of MODFLOW 6

By Alden M. Provost, Christian D. Langevin, and Joseph D. Hughes

Chapter 56 of
Section A, Groundwater
Book 6, Modeling Techniques

Prepared in cooperation with the U.S. Geological Survey Water Availability and Use Science Program

Techniques and Methods 6–A56

U.S. Department of the Interior
U.S. Geological Survey

U.S. Department of the Interior
RYAN K. ZINKE, Secretary

U.S. Geological Survey
William H. Werkheiser, Acting Director

U.S. Geological Survey, Reston, Virginia: 2017

Suggested citation:
Provost, A.M., Langevin, C.D., and Hughes, J.D., 2017, Documentation for the "XT3D" option in the Node Property Flow (NPF) Package of MODFLOW 6: U.S. Geological Survey Techniques and Methods, book 6, chap. A56, 40 p., https://doi.org/10.3133/tm6A56.

ISSN 2328-7055 (online)

Preface

This report describes the "XT3D" option in the Node Property Flow (NPF) Package of the Groundwater Flow Model for the U.S. Geological Survey (USGS) modular hydrologic simulation program, called MODFLOW 6. The MODFLOW 6 program can be be downloaded from the USGS for free. The performance of the XT3D option has been tested in a variety of applications. Future applications, however, might reveal errors that were not detected in the test simulations. Users are requested to send notification of any errors found in this model documentation report or in the model program to the MODFLOW contact listed on the Web page. Updates might be made to both the report and to the model program. Users can check for updates on the MODFLOW Web page (https://doi.org/10.5066/F76Q1VQV).

Acknowledgments

The U.S. Geological Survey Water Availability and Use Science Program provided financial support for the work documented herein. The authors are grateful for the constructive discussions and reviews provided by Allen Shapiro and Ward Sanford of the U.S. Geological Survey, and to Dick Yager, Dan Goode, Tom Reilly, and Daniel Feinstein of the U.S. Geological Survey; Steffen Mehl of California State University, Chico; and Sorab Panday of GSI Environmental for their participation in fruitful discussions of the XT3D method. Communications with Sorab were particularly helpful in shaping the conceptual basis for the XT3D method. The authors are also grateful to Dave Pollock of the U.S. Geological Survey for kindly providing MODPATH-generated particle tracks for example 3.

Contents

Figures

Tables

Blank page

Documentation for the "XT3D" Option in the Node Property Flow (NPF) Package of MODFLOW 6

By Alden M. Provost, Christian D. Langevin, and Joseph D. Hughes

Abstract

This report describes the "XT3D" option in the Node Property Flow (NPF) Package of MODFLOW 6. The XT3D option extends the capabilities of MODFLOW by enabling simulation of fully three-dimensional anisotropy on regular or irregular grids in a way that properly takes into account the full, three-dimensional conductivity tensor. It can also improve the accuracy of groundwater-flow simulations in cases in which the model grid violates certain geometric requirements. Three example problems demonstrate the use of the XT3D option to simulate groundwater flow on irregular grids and through three-dimensional porous media with anisotropic hydraulic conductivity.

Conceptually, the XT3D method of estimating flow between two MODFLOW 6 model cells can be viewed in terms of three main mathematical steps: construction of head-gradient estimates by interpolation; construction of fluid-flux estimates by application of the full, three-dimensional form of Darcy's Law, in which the conductivity tensor can be heterogeneous and anisotropic; and construction of the flow expression by enforcement of continuity of flow across the cell interface. The resulting XT3D flow expression, which relates the flow across the cell interface to the values of heads computed at neighboring nodes, is the sum of terms in which conductance-like coefficients multiply head differences, as in the conductance-based flow expression the NPF Package uses by default. However, the XT3D flow expression contains terms that involve "neighbors of neighbors" of the two cells for which the flow is being calculated. These additional terms have no analog in the conductance-based formulation. When assembled into matrix form, the XT3D formulation results in a larger stencil than the conductance-based formulation; that is, each row of the coefficient matrix generally contains more nonzero elements. The "RHS" suboption can be used to avoid expanding the stencil by placing the additional terms on the right-hand side of the matrix equation and evaluating them at the previous iteration or time step.

The XT3D option can be an alternative to the Ghost-Node Correction (GNC) Package. However, the XT3D formulation is typically more computationally intensive than the conductance-based formulation the NPF Package uses by default, either with or without ghost nodes. Before deciding whether to use the GNC Package or XT3D option for production runs, the user should consider whether the conductance-based formulation alone can provide acceptable accuracy for the particular problem being solved.

Introduction

This report describes the "XT3D" option in the Node Property Flow (NPF) Package of the Groundwater Flow (GWF) Model of MODFLOW 6 (Langevin and others, 2017). The XT3D option offers a new control-volume finite difference (CVFD) formulation for simulating groundwater flow in situations in which the principal directions of hydraulic conductivity are not aligned with the model grid. With the exception of the Model-Layer Variable-Direction Horizontal Anisotropy (LVDA) capability in the Hydrologic-Unit Flow (HUF) Package (Anderman and others, 2002), all previous versions of MODFLOW either required that the principal directions of conductivity be aligned with the model-grid connections or used an *ad hoc* approach to compute effective hydraulic conductivities along grid connections, as the NPF Package of MODFLOW 6 does by default. The LVDA capability took a more mathematically rigorous approach to handling anisotropy, but it was limited to variable-direction anisotropy within the horizontal plane. The XT3D option extends the capabilities of MODFLOW by enabling simulation of fully three-dimensional (3D) anisotropy on regular or irregular grids in a way that properly takes into account the full, three-dimensional conductivity tensor. Accordingly, the XT3D option allows for specification of principal hydraulic conductivities and principal-direction orientations that vary from cell to cell. The XT3D formulation can also improve the accuracy of groundwater-flow simulations in cases in which the model grid violates the CVFD geometric requirements discussed in the GWF Model documentation (Langevin and others, 2017) and summarized in this report. Thus, the XT3D option is an alternative to the Ghost-Node Correction (GNC) Package described by Panday and others (2013).

The purpose of this report is to describe the mathematical model of groundwater flow and the conceptual basis for the XT3D method; derive the XT3D flow expression and the corresponding CVFD equations; and discuss the features, applicability, and limitations of the XT3D option. Conceptually, the XT3D method of estimating flow between two model cells can be viewed in terms of three main mathematical steps: construction of head-gradient estimates by interpolation; construction of fluid-flux estimates by application of the full, three-dimensional form of Darcy's Law, in which the conductivity tensor can be heterogeneous and anisotropic; and construction of the flow expression by enforcement of continuity of flow across the cell interface. The derivation of the XT3D flow expression presents the details of the calculations in a way that parallels this three-step progression. Symbols are defined in appendix A.

Three example problems demonstrate the use of the XT3D option to simulate groundwater flow on irregular grids and through 3D porous media with anisotropic hydraulic conductivity. Input files for the example problems are included in the MODFLOW 6 software release. The input-data structure for the XT3D option is described in a separate User Guide that is distributed with the MODFLOW 6 software.

Mathematical Model of Groundwater Flow

Constant-density groundwater flow through a porous medium is described by Darcy's Law:

$$\mathbf{q} = -\mathbf{K}\boldsymbol{\nabla}h, \tag{1}$$

where $\mathbf{q}$ is a vector of specific discharge (L/T), or fluid-flux vector; $\mathbf{K}$ is the second-order hydraulic-conductivity tensor (L/T); h is hydraulic head (L); and $\boldsymbol{\nabla}h$ is the hydraulic-head gradient vector (dimensionless). As discussed in the GWF Model documentation (Langevin and others, 2017), the NPF Package assumes

by default that the principal axes of hydraulic conductivity are aligned with the global model-coordinate system (x, y, z), so that in the global model-coordinate system $\mathbf{K}$ is represented by a diagonal matrix:

$$\mathbf{K} = \begin{pmatrix} K_{xx} & 0 & 0 \\ 0 & K_{yy} & 0 \\ 0 & 0 & K_{zz} \end{pmatrix}, \tag{2}$$

where K_{xx}, K_{yy}, and K_{zz} are values of hydraulic conductivity (L/T) along the x, y, and z coordinate axes. Substitution of equation 2 into equation 1 yields

$$\begin{aligned} q_x &= -K_{xx}\frac{\partial h}{\partial x} \\ q_y &= -K_{yy}\frac{\partial h}{\partial y} \\ q_z &= -K_{zz}\frac{\partial h}{\partial z}. \end{aligned} \tag{3}$$

With the form of Darcy's Law given by equation 3, the volumetric balance equation for groundwater (see, for example, Rushton and Redshaw, 1979) is

$$\frac{\partial}{\partial x}\left(K_{xx}\frac{\partial h}{\partial x}\right) + \frac{\partial}{\partial y}\left(K_{yy}\frac{\partial h}{\partial y}\right) + \frac{\partial}{\partial z}\left(K_{zz}\frac{\partial h}{\partial z}\right) + Q'_s = S_S\frac{\partial h}{\partial t}, \tag{4}$$

where Q'_s is volumetric inflow or outflow of water per unit volume (T^{-1}), which is positive for sources and negative for sinks; S_S is the specific storage (L^{-1}); and t is time (T).

Chapters 2 and 4 of the GWF Model documentation (Langevin and others, 2017) describe in detail the formulation and solution of the Control-Volume Finite-Difference (CVFD) equations the NPF Package uses to approximate equation 4. The basis for those CVFD equations is the conductance-based flow expression, in which the flow between two cells is proportional to the head difference between their nodes:

$$Q_{n,m} = C_{n,m}\left(h_m - h_n\right), \tag{5}$$

where h_n and h_m are the heads computed at nodes n and m, respectively; $C_{n,m}$ is a positive conductance (L^2/T); and $Q_{n,m}$ (L^3/T) is the flow into cell n from cell m (which is negative if $h_n > h_m$). Equation 5 can provide an accurate estimate of the flow if the model grid is regular and the principal directions of $\mathbf{K}$ coincide with the grid-aligned global model-coordinate system, or if an irregular grid satisfies certain geometric requirements and $\mathbf{K}$ is isotropic ($K_{xx} = K_{yy} = K_{zz}$). Chapter 2 of the GWF Model documentation (Langevin and others, 2017) defines regular and irregular grids and discusses the geometric requirements an irregular grid must obey for equation 5 to be accurate. These requirements are also summarized in the section of this report titled "Applicability and Limitations of the 'XT3D' Option."

When the hydraulic conductivity is anisotropic and the orientation of the principal axes varies spatially, $\mathbf{K}$ cannot be expressed in diagonal form with respect to the global model-coordinate system throughout the entire model domain. In that case, the most general form of $\mathbf{K}$, which is symmetric, is

$$\mathbf{K} = \begin{pmatrix} K_{xx} & K_{xy} & K_{xz} \\ K_{xy} & K_{yy} & K_{yz} \\ K_{xz} & K_{yz} & K_{zz} \end{pmatrix}, \tag{6}$$

where K_{xy}, K_{xz}, K_{yx}, K_{yz}, K_{zx}, and K_{zy} (L/T) are "off-diagonal" elements. Substitution of equation 6 into equation 1 yields:

$$\begin{aligned} q_x &= -K_{xx}\frac{\partial h}{\partial x} - K_{xy}\frac{\partial h}{\partial y} - K_{xz}\frac{\partial h}{\partial z} \\ q_y &= -K_{xy}\frac{\partial h}{\partial x} - K_{yy}\frac{\partial h}{\partial y} - K_{yz}\frac{\partial h}{\partial z} \\ q_z &= -K_{xz}\frac{\partial h}{\partial x} - K_{yz}\frac{\partial h}{\partial y} - K_{zz}\frac{\partial h}{\partial z} \end{aligned} \tag{7}$$

(see, for example, Freeze and Cherry, 1979). With the form of Darcy's Law given by equation 7, instead of equation 3, the volumetric balance equation for groundwater takes the more general form

$$\begin{aligned} \frac{\partial}{\partial x}\left(K_{xx}\frac{\partial h}{\partial x} + K_{xy}\frac{\partial h}{\partial y} + K_{xz}\frac{\partial h}{\partial z}\right) + \frac{\partial}{\partial y}\left(K_{xy}\frac{\partial h}{\partial x} + K_{yy}\frac{\partial h}{\partial y} + K_{yz}\frac{\partial h}{\partial z}\right) \\ + \frac{\partial}{\partial z}\left(K_{xz}\frac{\partial h}{\partial x} + K_{yz}\frac{\partial h}{\partial y} + K_{zz}\frac{\partial h}{\partial z}\right) + Q'_s = S_S\frac{\partial h}{\partial t}. \end{aligned} \tag{8}$$

If $\mathbf{K}$ is anisotropic and its principal directions are not everywhere aligned with the grid, either because the principal directions vary spatially on a regular grid or because the grid is irregular, then equation 5 is insufficient to provide an accurate estimate of the flow. Accurate estimation of the flow must then be based on an estimate of the entire, 3D head-gradient vector, not just on a single component of the head gradient. This, in turn, requires head information from additional neighboring nodes. The resulting flow expression necessarily includes terms that are not included in equation 5.

The XT3D method is designed to handle fully three-dimensional anisotropy in cases in which the principal directions are not everywhere aligned with the grid. It is based on a particular approach to incorporating neigboring head information to construct an estimate of the head-gradient vector. The XT3D method is also useful in cases in which an irregular grid fails to satisfy the requisite geometric constraints for maintaining the accuracy of equation 5. When the XT3D option is active, the NPF Package uses an appropriately "extended" flow expression, which involves additional conductance-like coefficients, to compute flows between cells.

Conceptual Basis for the XT3D Method

The XT3D method produces an expression for the flow between two model cells, n and m, as a function of the heads in those two cells and their neighbors. Conceptually, the method is the result of three main mathematical steps:

1. On each side of the interface between cells n and m, construction of an expression for the head-gradient vector. The expression for the "cell n" side is a function of the heads in cell n and its neighbors, and an unknown head at the interface. The expression for the "cell m" side is a function of the heads in cell m and its neighbors, and the unknown head at the interface.

2. On each side of the interface between cells n and m, application of Darcy's Law (eq. 1) and calculation of an expression for the component of the fluid flux normal to the interface in terms of the heads mentioned above. $\mathbf{K}$ can be anisotropic and different on each side of the interface.

3. Application of the continuity principle, which requires that the flow crossing the interface between cells n and m be the same on each side of the interface. This allows the unknown head at the interface to be solved for and leads to a single expression for the flow across the interface in terms of the heads in cells n and m and their neighbors.

Estimation of the gradient vector, as in step 1, is the basis for so-called "gradient-reconstruction" methods, which incorporate gradient information from neighboring cells. Gradient reconstruction methods for estimating gradients at cell interfaces of cell-centered grids include "node-averaging" schemes and "least-square" schemes (see, for example, Diskin and Thomas, 2011). In node-averaging schemes, values of head (or other solution variable whose gradient is to be estimated) at cell centers are interpolated at the cell vertices (often called "nodes" in the literature), and gradient estimates are constructed using values at the vertices. Least-square schemes estimate the gradient by minimizing the weighted sum of squared errors in heads or head-gradient components at neighboring points (Mavriplis, 2003; Diskin and Thomas, 2008). Weighting is typically based on distance between the neighboring point and the point at which the gradient estimate is desired, with smaller distance yielding greater weight.

The following concepts form the conceptual basis for the XT3D method:

- the use of weighted averaging to incorporate gradient information from neighboring connections,
- dependence of weights on distances and orientations, and
- combining information from both sides of the interface.

Figure 1 shows the connections used by the XT3D method to estimate the head gradient at the interface between two cells, n and its neighbor m, on an unstructured grid. (Although the grid shown in figure 1 consists of regular hexagons, the XT3D method is applicable to more general unstructured grids, as well.) In this context, the connection between cells n and m is the "primary connection," and the corresponding interface is the "primary interface." The gradient is estimated at the point at which the primary connection intersects the primary interface, which is marked with an "X." The component of the gradient along the primary connection is estimated simply by differencing along the primary connection. An obvious approach would be to difference over the entire length of the primary connection; that is, between the nodes n and m. Instead, an "unknown" head value is temporarily assigned to the point on the primary interface, and differencing along the primary connection is performed between node n and the interface, and between node m and the interface. The unknown head is eventually eliminated as a variable by enforcing continuity of the normal flux at the primary interface.

Estimation of the component of the head gradient perpendicular to the primary connection involves gathering and integrating information about the perpendicular component from the neighboring connections, drawn in orange and blue in figure 1. If the head gradient is perfectly uniform in the vicinity of cells n and m, then all neighboring connections provide mutually consistent information, and the perpendicular component of the gradient at the primary interface can be calculated exactly. In general, however, the gradient is not uniform. To accommodate nonuniformity of the gradient, information from each neighboring connection is weighted

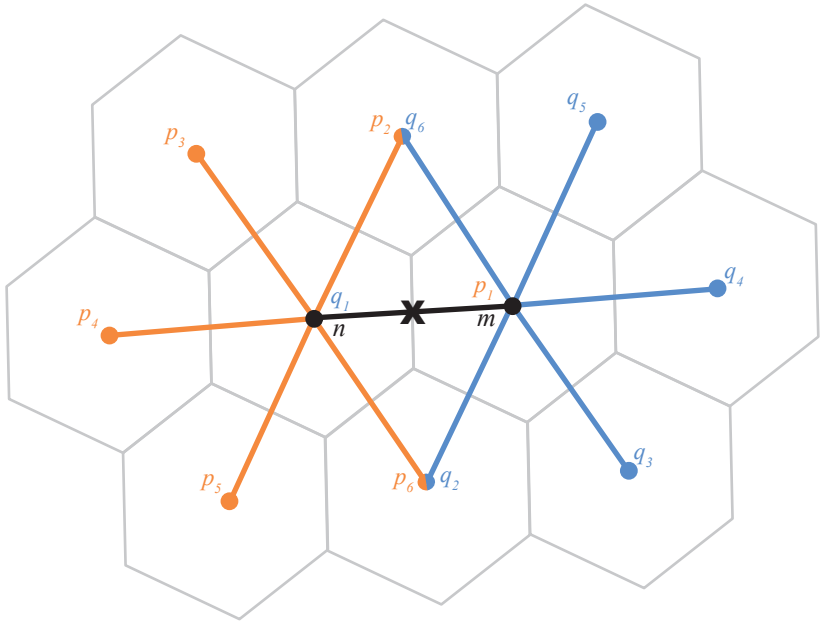

Figure 1. Diagram showing, in two dimensions, the connections used by the XT3D method to estimate the head gradient at a point ("X") on the interface between cells n and m (the "primary" interface). A separate estimate of the head gradient at point X is formulated using information from each side of the primary interface. On the "node n" side of the primary interface, the component of the gradient along the primary connection (black line) is estimated by finite differencing the heads at node n and point X, and the component of the gradient perpendicular to the primary connection is estimated using gradient-component information from connections between node n and its neighbors p_2, ..., p_6 (orange lines). An analogous procedure involving node m and its connections with its neighbors q_2, ..., q_6 (blue lines) is used to formulate an estimate of the head gradient for the "node m" side of the primary interface.

according to how close the connection is to the primary interface and how closely aligned the connection is with the direction perpendicular to the primary connection. In figure 1, unit vectors oriented along connections p_2 and p_3 have components of equal magnitude in the direction perpendicular to the primary connection, so orientation favors neither connection in this case. However, the midpoint of connection p_2 is closer to the primary interface than the midpoint of connection p_3, so connection p_2 receives a greater weight. Connection p_4 is parallel to the primary connection, so it provides no information about the perpendicular component of the gradient and, therefore, receives a weight of zero.

An estimate of the head-gradient vector on the "cell n" side of the primary interface is constructed by combining the estimate of the component along the primary connection with a weighted average of the perpendicular-component information provided by each of the neighboring connections of cell n. The resulting estimate of the gradient vector is expressed in terms of head values at neighbors of cell n and the "unknown" head value at the primary interface. A second estimate of the head-gradient vector is constructed similarly on the "cell m" side of the primary interface.

Having estimated the head-gradient vector on each side of the primary interface, one can compute the flow vector on each side of the primary interface using Darcy's Law, equation 1. Multiplying each of these two flow vectors by the interfacial area and computing the component of each vector in the direction normal to the primary interface, which need not be aligned with the primary connection, one then arrives at two estimates of the flow across the interface; that is, the internal flow, between cells n and m. As each of these two flow estimates involves the "unknown" head at the primary interface, the unknown head is chosen such that the two internal-flow estimates are equal, as required by continuity. The result is the XT3D flow expression, which is used to compute flows between cells in the Control-Volume Finite-Difference (CVFD) equations that approximate groundwater flow, as explained in the section "XT3D Control-Volume Finite-Difference (CVFD) Equation."

XT3D Flow Expression

As explained in the preceding section, the XT3D flow expression is the result of three main mathematical steps:

(1) construction of head-gradient vector expressions on each side of the primary interface by averging gradient information from neighboring connections,

(2) construction of normal-flux expressions on each side of the primary interface by applying Darcy's Law and calculating the normal component of the fluid flux, and

(3) construction of the flow expression by equating normal fluxes on each side of the primary interface.

The mathematical details underlying these main steps are presented in this section.

In the development below, $\boldsymbol{\gamma}$ represents head-gradient vectors, and $\mathbf{c}$ represents unit vectors that indicate connection orientation. An expression is developed for the flow between two cells, n and m, which meet at the "primary interface" and whose nodes are connected by the "primary connection." The connection between node n and its neighbor p is called connection (n, p). Associated with each connection is a Cartesian coordinate system: the coordinate axis along connection (n, p) is called the $x_{n,p}$ axis, and the two axes perpendicular to that connection are called the $y_{n,p}$ and $z_{n,p}$ axes. The gradient-estimation calculations described in this section are done primarily in the (x_1, y_1, z_1) coordinate system; that is, coordinates associated with the primary connection. Because coordinates x_1, y_1, and z_1 appear frequently in the equations, they are represented by x_1, y_1, and z_1, respectively, to simplify the notation. Except when stated otherwise, superscripts indicate vector components, and subscripts indicate cell connections: for example, $c^{x_1}_{n,p}$ is the x_1 component of the orientation vector for the primary connection. Figure 2 illustrates vectors, distances, and coordinates associated with the primary and neighboring connections. Symbols are defined in appendix A.

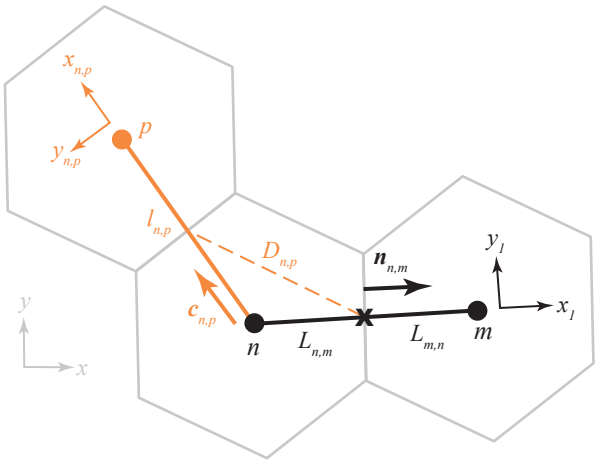

Figure 2. Diagram showing vectors, distances, and coordinates used in the mathematical development of the XT3D method. The distances from nodes n and m to the primary interface, measured along the primary connection (black line), are $L_{n,m}$ and $L_{m,n}$, respectively. The length of neighboring connection (n, p) (solid orange line) is $l_{n,p}$. The distance from the midpoint of connection (n, p) to the point (marked with a bold "X") where the primary connection intersects the primary interface is $D_{n,p}$ (dashed orange line). The unit connection-orientation vector for connection (n, p) is $\mathbf{c}_{n,p}$. The unit vector normal to the primary interface is $\mathbf{n}_{n,m}$. Model-cooordinate axes are show in gray, local-coordinate axes associated with the primary connection are shown in black, and local-coordinate axes associated with connection (n, p) are shown in orange.

Vectors are defined as column vectors by default. Thus, the transpose of a vector $\mathbf{u}$, denoted $\mathbf{u}^T$, is a row vector, and $\mathbf{u}^T\mathbf{v}$ denotes the scalar product ("dot" product) of vectors $\mathbf{u}$ and $\mathbf{v}$. Units of length and time are denoted by "(L)" and "(T)," respectively.

Construction of Head-Gradient Vector Expressions on Each Side of the Primary Interface

Consider the information supplied by connection (n, p). By finite differencing across the connection, one can estimate the component of the head gradient along the connection, which is denoted as $\gamma_{n,p}^{x_{n,p}}$. The superscript $x_{n,p}$ denotes the fact that this is the component along the $x_{n,p}$ direction. If $c_{n,p}$ is the connection-orientation vector for connection (n, p) and $\gamma_{n,p}$ is the head-gradient vector at interface (n, p), then by definition

$$\mathbf{c}_{n,p}^T \boldsymbol{\gamma}_{n,p} = \gamma_{n,p}^{x_{n,p}}, \tag{9}$$

or, with the vectors expressed in (x_1, y_1, z_1) coordinates; that is, coordinates associated with the primary connection,

$$c_{n,p}^{x_1}\gamma_{n,p}^{x_1} + c_{n,p}^{y_1}\gamma_{n,p}^{y_1} + c_{n,p}^{z_1}\gamma_{n,p}^{z_1} = \gamma_{n,p}^{x_{n,p}}. \tag{10}$$

Now, suppose one is interested in estimating the y_1 component of the gradient (one of the two perpendicular components relative to the primary connection) at interface (n, p). Solving equation 10 for that component gives

$$\gamma_{n,p}^{y_1} = \left(\gamma_{n,p}^{x_{n,p}} - c_{n,p}^{x_1}\gamma_{n,p}^{x_1} - c_{n,p}^{z_1}\gamma_{n,p}^{z_1}\right)/c_{n,p}^{y_1}. \tag{11}$$

On the right-hand side of equation 11, $\gamma_{n,p}^{x_{n,p}}$ can be obtained by finite-differencing across the connection (n, p), but $\gamma_{n,p}^{x_1}$ and $\gamma_{n,p}^{z_1}$, the x_1 and z_1 components at interface (n, p), are unknown. If it is assumed that the latter can be approximated by their counterparts at interface (n, m), $\gamma_{n,m}^{x_1}$ and $\gamma_{n,m}^{z_1}$, then

$$\gamma_{n,p}^{y_1} = \left(\gamma_{n,p}^{x_{n,p}} - c_{n,p}^{x_1}\gamma_{n,m}^{x_1} - c_{n,p}^{z_1}\gamma_{n,m}^{z_1}\right)/c_{n,p}^{y_1}. \tag{12}$$

Equation 12 provides an estimate of the y_1 component of the gradient based on information from connection (n, p). Weighted averaging of the estimates from all the nonprimary connections of cell n gives

$$\gamma_{n,m}^{y_1} = \sum_{\substack{p\in\eta_n \\ p\neq m}} \varphi_{n,p}^{y_1}\gamma_{n,p}^{y_1} = \sum_{\substack{p\in\eta_n \\ p\neq m}} \frac{\varphi_{n,p}^{y_1}\gamma_{n,p}^{x_{n,p}}}{c_{n,p}^{y_1}} - \left(\sum_{\substack{p\in\eta_n \\ p\neq m}} \frac{\varphi_{n,p}^{y_1}c_{n,p}^{x_1}}{c_{n,p}^{y_1}}\right)\gamma_{n,m}^{x_1} - \left(\sum_{\substack{p\in\eta_n \\ p\neq m}} \frac{\varphi_{n,p}^{y_1}c_{n,p}^{z_1}}{c_{n,p}^{y_1}}\right)\gamma_{n,m}^{z_1}, \tag{13}$$

where the summations are over the neighbors (connections) of cell n, excluding cell m, and $\varphi_{n,p}^{y_1}$ is the weight assigned to the estimate from connection (n, p). Assignment of weights is discussed in detail later.

Equation 13 was derived for the y_1 component of the gradient, and an analogous equation can be derived for the z_1 component. The result is a system of two equations that can be solved for $\gamma_{n,m}^{y_1}$ and $\gamma_{n,m}^{z_1}$:

$$\begin{aligned}
\gamma_{n,m}^{y_1} &= -\alpha^{y_1}\gamma_{n,m}^{x_1} + \sum_{\substack{p\in\eta_n \\ p\neq m}} \beta_{n,p}^{y_1}\gamma_{n,p}^{x_{n,p}} \\
\gamma_{n,m}^{z_1} &= -\alpha^{z_1}\gamma_{n,m}^{x_1} + \sum_{\substack{p\in\eta_n \\ p\neq m}} \beta_{n,p}^{z_1}\gamma_{n,p}^{x_{n,p}},
\end{aligned} \tag{14}$$

where

$$\begin{aligned}
\alpha^{y_1} &= \frac{A^{x_1y_1} - A^{x_1z_1}A^{z_1y_1}}{1 - A^{y_1z_1}A^{z_1y_1}} \\
\alpha^{z_1} &= \frac{A^{x_1z_1} - A^{x_1y_1}A^{y_1z_1}}{1 - A^{y_1z_1}A^{z_1y_1}} \\
\beta_{n,p}^{y_1} &= \frac{B_{n,p}^{y_1} - B_{n,p}^{z_1}A^{z_1y_1}}{1 - A^{y_1z_1}A^{z_1y_1}} \\
\beta_{n,p}^{z_1} &= \frac{B_{n,p}^{z_1} - B_{n,p}^{y_1}A^{y_1z_1}}{1 - A^{y_1z_1}A^{z_1y_1}},
\end{aligned} \tag{15}$$

and

$$A^{uv} = \sum_{\substack{p \in \eta_n \\ p \neq m}} \frac{\varphi^v_{n,p} c^u_{n,p}}{c^v_{n,p}} = \sum_{\substack{p \in \eta_n \\ p \neq m}} B^v_{n,p} c^u_{n,p}$$
$$B^v_{n,p} = \frac{\varphi^v_{n,p}}{c^v_{n,p}}, \tag{16}$$

where superscript u can take on values of x_1, y_1, and z_1, and superscript v can take on values of y_1 and z_1.

The weighting scheme is designed to place the greatest weight on connections that are located closest to the primary interface and most closely aligned with the perpendicular direction of interest. Each weight must also go to zero faster than $c^v_{n,p}$ to keep $B^v_{n,p}$ in equation 16 from becoming infinite, and the weights must collectively sum to 1. These requirements are satisfied by the following weights:

$$\varphi^v_{n,p} = \frac{\omega^v_{n,p} \left| c^v_{n,p} \right|}{\sum_{\substack{l \in \eta_n \\ l \neq m}} \omega^v_{n,l} \left| c^v_{n,l} \right|}, \tag{17}$$

where

$$\omega^v_{n,p} = \left(1 - \frac{D_{n,p} \left| c^v_{n,p} \right|}{\sum_{\substack{l \in \eta_n \\ l \neq m}} D_{n,l} \left| c^v_{n,l} \right|} \right) \left| c^v_{n,p} \right|. \tag{18}$$

Distance $D_{n,p}$ is measured from the midpoint of connection (n, p) to the point at which the gradient is being estimated; that is, the point at which the primary connection intersects the primary interface.

Estimates of all three components of the gradient vector at interface (n, m) have now been constructed for the cell n side of the primary interface. Component $\gamma^{x_1}_{n,m}$ is estimated directly by finite differencing along the primary connection, and $\gamma^{y_1}_{n,m}$ and $\gamma^{z_1}_{n,m}$ are estimated using equation 14. Identical expressions apply to the cell m side of the primary interface, but with "n" and "m" exchanging roles, and with summations performed over the neighbors of cell m.

Construction of Flow Expressions on Each Side of the Primary Interface

With the head-gradient vector having been estimated on the cell n side of the interface, the conductivity tensor can now be applied to get the flux vector. The flux component normal to the interface can then be calculated. If $\mathbf{K}_n$ is the conductivity tensor for cell n and $\mathbf{n}_{n,m}$ is the unit normal vector (oriented outward from cell n) for interface (n, m), then the normal flux into cell n at interface (n, m) is given by

$$q_{n,m} = \left(-\mathbf{n}^T_{n,m} \right) \left(-\mathbf{K}_n \boldsymbol{\gamma}_{n,m} \right) = \mathbf{n}^T_{n,m} \mathbf{K}_n \boldsymbol{\gamma}_{n,m}. \tag{19}$$

Note that in the previous section the components of the gradient $\boldsymbol{\gamma}_{n,m}$ were computed in (x_1, y_1, z_1) coordinates. Assuming the conductivity tensor and normal vectors are supplied by the user in model coordinates

(x, y, z), the components of $\boldsymbol{\gamma}_{n,m}$ need to be transformed from (x_1, y_1, z_1) to (x, y, z) coordinates. Equation 19 can then be expanded and rearranged to read

$$q_{n,m} = a_{n,m}\,\gamma_{n,m}^{x_1} + \sum_{\substack{p\in\eta_n \\ p\neq m}} b_{n,p,(n,m)}\,\gamma_{n,p}^{x_{n,p}}, \tag{20}$$

where

$$\begin{aligned} a_{n,m} &= \sigma^{x_1} - \sigma^{y_1}\alpha^{y_1} - \sigma^{z_1}\alpha^{z_1} \\ b_{n,p,(n,m)} &= \sigma^{y_1}\beta_{n,p}^{y_1} + \sigma^{z_1}\beta_{n,p}^{z_1} \end{aligned} \tag{21}$$

and

$$\boldsymbol{\sigma} = \mathbf{n}_{n,m}^{T}\mathbf{K}_n\,\mathbf{R}, \tag{22}$$

where $\mathbf{R}$ is the coordinate-transformation (rotation) matrix. In coordinate system (x_1, y_1, z_1), the x_1 axis is, by definition, aligned with connection-orientation vector $c_{n,m}$. However, one is free to choose any y_1 and z_1 axes that are perpendicular to x_1 and to each other, and which coincide with the y and z axes on a rectilinear grid. This can be accomplished by considering the (x_1, y_1, z_1) axes as a rotation of the (x, y, z) axes by angle θ_1 within the (x, y) plane (counterclockwise as viewed looking down the z axis toward the origin), then by angle θ_2 up out of the (x, y) plane, such that a unit vector initially aligned with the x axis is mapped to $\mathbf{c}_{n,m}$. The corresponding rotation matrix that transforms vectors from (x_1, y_1, z_1) back to (x, y, z) coordinates (the matrix $\mathbf{R}$) is

$$\mathbf{R} = \begin{pmatrix} C_1C_2 & C_1S_2S_3 - S_1C_3 & -C_1S_2C_3 - S_1S_3 \\ S_1C_2 & S_1S_2S_3 + C_1C_3 & -S_1S_2C_3 + C_1S_3 \\ S_2 & -C_2S_3 & C_2C_3 \end{pmatrix}, \tag{23}$$

where

$$\begin{aligned} S_1 &= c_{n,m}^{y} \Big/ \sqrt{1 - \left(c_{n,m}^{z}\right)^2} \\ C_1 &= c_{n,m}^{x} \Big/ \sqrt{1 - \left(c_{n,m}^{z}\right)^2} \\ S_2 &= c_{n,m}^{z} \\ C_2 &= \sqrt{1 - \left(c_{n,m}^{z}\right)^2} \\ S_3 &= 0 \\ C_3 &= 1. \end{aligned} \tag{24}$$

In the limit as $\mathbf{c}_{n,m}$ becomes vertical ($\theta_2 = \pm 90^\circ$; $c_{n,m}^{z} = \pm 1$), one can simply set $S_1 = 0$, $C_1 = 1$, $S_2 = \pm 1$, and $C_2 = 0$.

Equation 20 gives the normal flux in terms of finite differences across the various connections of cell n, which can be written in terms of heads as

$$\begin{aligned} \gamma_{n,m}^{x_1} &= \frac{h_{n,m}^{*} - h_n}{L_{n,m}} \\ \gamma_{n,p}^{x_1} &= \frac{h_p - h_n}{l_{n,p}}, \end{aligned} \tag{25}$$

where h_p is the head at node p, and $l_{n,p}$ is the length of connection (n, p). For the primary connection, (n, m), the finite differencing is done between cell n and the primary interface. The symbol $h_{n,m}^{*}$ represents the head at the primary interface, which will be eliminated when the normal fluxes on both sides of the interface are equated in the next section, and $L_{n,m}$ is the distance between the center of cell n and the primary interface. Substitution of equation 25 into equation 20, rearrangement, and multiplication by the area of the primary interface associated with cell n, $A_{n,m}$, then gives an expression for the flow into cell n from cell m:

$$Q_{n,m} = q_{n,m} A_{n,m} = -\left(\hat{a}_{n,m} + \sum_{\substack{p \in \eta_n \\ p \neq m}} \hat{b}_{n,p,(n,m)} \right) h_n + \hat{a}_{n,m}\, h_{n,m}^{*} + \sum_{\substack{p \in \eta_n \\ p \neq m}} \hat{b}_{n,p,(n,m)}\, h_p, \tag{26}$$

where

$$\begin{aligned} \hat{a}_{n,m} &= a_{n,m} A_{n,m} / L_{n,m} \\ \hat{b}_{n,p,(n,m)} &= b_{n,p,(n,m)} A_{n,m} / l_{n,p}. \end{aligned} \tag{27}$$

Following the procedure used by the NPF Package when calculating harmonic-mean transmissivities (Langevin and others, 2017), XT3D bases the interfacial area associated with a cell on the saturated thickness of the cell.

Equation 26 provides an estimate of the flow computed on the cell n side of the primary interface. An analogous expression applies to the cell m side of the primary interface:

$$Q_{m,n} = q_{m,n} A_{m,n} = -\left(\hat{a}_{m,n} + \sum_{\substack{q \in \eta_m \\ q \neq n}} \hat{b}_{m,q,(m,n)} \right) h_m + \hat{a}_{m,n}\, h_{m,n}^{*} + \sum_{\substack{q \in \eta_m \\ q \neq n}} \hat{b}_{m,q,(m,n)}\, h_q, \tag{28}$$

where $\hat{a}_{m,n}$ and $\hat{b}_{m,q,(m,n)}$ are again defined by equation 27, but with "n" and "m" exchanging roles, and with "q" taking the place of "p."

Construction of the XT3D Flow Expression

Continuity demands that the flow into cell m from cell n be equal and opposite in sign to the flow into cell n from cell m:

$$Q_{m,n} = -Q_{n,m}, \tag{29}$$

In this development, the primary interface is assumed not to provide any resistance to flow beyond what the cells themselves provide. In that case, the same interfacial head value applies to both sides of the primary interface; that is,

$$h^*_{n,m} - h^*_{m,n} = 0. \tag{30}$$

Multiplication of equation 26 by $\hat{a}_{m,n}$ and equation 28 by $\hat{a}_{n,m}$, subtraction of the two resulting equations, elimination of $Q_{m,n}$ and $h^*_{n,m} - h^*_{m,n}$ using equations 29 and 30, respectively, and solution for $Q_{n,m}$ then gives the XT3D flow expression

$$Q_{n,m} = C_{n,m,(n,m)} \left(h_m - h_n\right) + \sum_{\substack{p \in \eta_n \\ p \neq m}} C_{n,p,(n,m)} \left(h_p - h_n\right) - \sum_{\substack{q \in \eta_m \\ q \neq n}} C_{m,q,(n,m)} \left(h_q - h_m\right), \tag{31}$$

where the conductance-like coefficients are defined as

$$\begin{aligned} C_{n,m,(n,m)} &= \frac{\hat{a}_{n,m}\hat{a}_{m,n}}{\hat{a}_{n,m} + \hat{a}_{m,n}} \\ C_{n,p,(n,m)} &= \frac{\hat{a}_{m,n}\hat{b}_{n,p,(n,m)}}{\hat{a}_{n,m} + \hat{a}_{m,n}} \\ C_{m,q,(n,m)} &= \frac{\hat{a}_{n,m}\hat{b}_{m,q,(n,m)}}{\hat{a}_{n,m} + \hat{a}_{m,n}}. \end{aligned} \tag{32}$$

The XT3D flow expression is "extended" relative to the conductance-based flow expression (eq. 5) in that it involves not only the head difference between cells n and m, but also head differences between cell n and each of its neighbors other than m, which appear in the first summation, and between cell m and each of its neighbors other than n, which appear in the second summation. The "C" coefficients have units of conductance and each involve three subscripts. The first two subscripts indicate the two heads to which the coefficient applies. The third subscript, which is a pair of cell numbers, indicates the two cells between which flow is being calculated. For example, $C_{n,p,(n,m)}$ is the coefficient applied to the difference between heads h_p and h_n in the flow expression for the interface between cells n and m. The form of the XT3D flow expression on a rectangular grid is derived in appendix B.

XT3D Control-Volume Finite-Difference (CVFD) Equation

As discussed in the documentation for the GWF Model (Langevin and others, 2017), the continuity equation expressing the balance of constant-density groundwater flow, or "water balance," for cell n may be written as

$$\sum_{m \in \eta_n} Q_{n,m} + P_n h_n + Q_n = SS_n \Delta V_n \frac{h_n - HOLD_n}{t - t_{old}}, \tag{33}$$

where $HOLD_n$ and h_n are the heads (L) at node n at the beginning and end of the current time step, respectively; t_{old} and t are beginning and ending times (T) for the time step, respectively; SS_n is the specific storage

(L^{-1}) of cell n; and $P_n h_n + Q_n$ represents flows (L^3T^{-1}) into and out of cell n due to external sources and sinks. Substitution of equation 31 into equation 33 gives the XT3D CVFD equation for cell n:

$$\sum_{m \in \eta_n} C_{n,m,(n,m)} \left(h_m - h_n\right) + \sum_{m \in \eta_n} \sum_{\substack{p \in \eta_n \\ p \neq m}} C_{n,p,(n,m)} \left(h_p - h_n\right) - \sum_{m \in \eta_n} \sum_{\substack{q \in \eta_m \\ q \neq n}} C_{m,q,(n,m)} \left(h_q - h_m\right) + P_n h_n^m + Q_n = SS_n \Delta V_n \frac{h_n - HOLD_n}{t - t_{old}}, \tag{34}$$

which can be rearranged to the following form:

$$\sum_{m \in \eta_n} \left(\sum_{p \in \eta_n} C_{n,m,(n,p)} \right) \left(h_m - h_n\right) + \sum_{m \in \eta_n} \sum_{\substack{q \in \eta_m \\ q \neq n}} C_{m,q,(n,m)} \left(h_q - h_m\right) + P_n h_n + Q_n = SS_n \Delta V_n \frac{h_n - HOLD_n}{t - t_{old}}. \tag{35}$$

Equation 35 is similar in form to the conductance-based CVFD equation, except for the second term in equation 35, which has no analog in the conductance-based CVFD equation. This additional term incorporates head information from the neighbors, q, of each of the neighbors, m, of cell n, thereby extending the stencil of the CVFD equation beyond the immediate neighbors of cell n.

XT3D Formulation of the CVFD Equation for Solution

Rearrangement of equation 35 gives the XT3D formulation of the CVFD equation:

$$\sum_{m \in \eta_n} \left[\sum_{p \in \eta_n} C_{n,m,(n,p)} h_m - \sum_{\substack{q \in \eta_m \\ q \neq n}} C_{m,q,(n,m)} \left(h_q - h_m\right) \right] - \left[\sum_{m \in \eta_n} \left(\sum_{p \in \eta_n} C_{n,m,(n,p)} \right) + HCOF_n - \frac{SS_n \Delta V_n}{t - t_{old}} \right] h_n = RHS_n, \tag{36}$$

where

$$HCOF_n = P_n, \tag{37}$$

and

$$RHS_n = -Q_n - SS_n \Delta V_n \frac{HOLD_n}{t - t_{old}}. \tag{38}$$

An alternative formulation places terms involving interactions between neighbor m and its neighbors other than n on the right-hand side:

$$\sum_{m\in\eta_n}\sum_{p\in\eta_n} C_{n,m,(n,p)}h_m - \left[\sum_{m\in\eta_n}\left(\sum_{p\in\eta_n} C_{n,m,(n,p)}\right) + HCOF_n - \frac{SS_n\Delta V_n}{t-t_{old}}\right]h_n = RHS_n^*, \tag{39}$$

where

$$RHS_n^* = RHS_n + \sum_{\substack{q\in\eta_m \\ q\neq n}} C_{m,q,(n,m)}\left(h_q - h_m\right), \tag{40}$$

and terms in RHS_n^* are evaluated at the previous iteration or time step. The formulation in equation 39 requires less computer memory and less computational effort per iteration than the formulation in equation 36, but overall it may require more iterations, and therefore more computational effort. Also, equation 39 is similar in form to the conductance-based CVFD equation and has the same stencil, that is, it includes the same heads as "unknowns" to solve for on the left-hand side of the equation.

As is done for the conductance-based CVFD equations, the XT3D CVFD equations (36 or 39) for all cells in the model are assembled into matrix form for solution:

$$\mathbf{Ah} = \mathbf{q}. \tag{41}$$

$\mathbf{A}$ is the coefficient matrix, which is assembled from "C" coefficients from the left-hand side of equation 36 or 39, $\mathbf{h}$ is the vector of nodal head values being solved for at the end of the time step, and $\mathbf{q}$ is a vector of constant terms from the right-hand side of equation 36 or 39.

Newton-Raphson Formulation of the XT3D CVFD Equation for Solution

The NPF Package of MODFLOW 6 (Langevin and others, 2017) includes a Newton-Raphson-formulation option that can improve model convergence for highly nonlinear problems, such as some problems involving water-table conditions. The Newton-Raphson formulation for the XT3D flow expression is comparable to the Newton-Raphson formulation for the standard conductance-based flow expression used by default in the NPF Package (eq. 4–32 in Langevin and others, 2017). Differentiation of the XT3D flow expression, equation 31, with respect to h_n gives

$$\begin{aligned}\frac{\partial Q_{n,m}}{\partial h_n} = &- C_{n,m,(n,m)} + \frac{\partial C_{n,m,(n,m)}}{\partial h_n}\left(h_m - h_n\right) \\ &- \sum_{\substack{p\in\eta_n \\ p\neq m}} C_{n,p,(n,m)} + \sum_{\substack{p\in\eta_n \\ p\neq m}} \frac{\partial C_{n,p,(n,m)}}{\partial h_n}\left(h_p - h_n\right) - \sum_{\substack{q\in\eta_m \\ q\neq n}} \frac{\partial C_{m,q,(n,m)}}{\partial h_n}\left(h_q - h_m\right).\end{aligned} \tag{42}$$

When the Newton-Raphson formulation is invoked, upstream weighting is used (Langevin and others, 2017). If h_n is the upstream head, the interfacial area $A_{n,m}$ is used on both sides of the primary interface; that is, $A_{m,n} = A_{n,m}$. Furthermore, $A_{n,m}$ is calculated as

$$A_{m,n} = {S_{F_n}}^* \Delta v_n^0 \Delta w_{n,m}, \tag{43}$$

where ${S_{F_n}}^*$ is the smoothed saturated fraction of cell n defined in Chapter 4 of Langevin and others (2017), Δv_n^0 is the thickness of cell n (fully saturated), and $\Delta w_{n,m}$ is the width of the primary interface. Examination of equations 27, 32, and 43 shows that the conductance-like coefficients in equation 42 are then each proportional to ${S_{F_n}}^*$:

$$\begin{aligned} C_{n,m,(n,m)} &= C^0_{n,m,(n,m)} {S_{F_n}}^* \\ C_{n,p,(n,m)} &= C^0_{n,p,(n,m)} {S_{F_n}}^* \\ C_{m,q,(n,m)} &= C^0_{m,q,(n,m)} {S_{F_n}}^*, \end{aligned} \tag{44}$$

where $C^0_{n,m,(n,m)}$, $C^0_{n,p,(n,m)}$, and $C^0_{m,q,(n,m)}$ are the values of $C_{n,m,(n,m)}$, $C_{n,p,(n,m)}$, and $C_{m,q,(n,m)}$, respectively, at full saturation. Differentiation of each of the three conductance-like coefficient in equation 44 with respect to ${S_{F_n}}^*$, substitution into equation 42, and rearrangement then gives

$$\begin{aligned} \frac{\partial Q_{n,m}}{\partial h_n} &= -C_{n,m,(n,m)} - \sum_{\substack{p \in \eta_n \\ p \neq m}} C_{n,p,(n,m)} \\ &+ \frac{d{S_{F_n}}^*}{dh_n} \left[C^0_{n,m,(n,m)} (h_m - h_n) + \sum_{\substack{p \in \eta_n \\ p \neq m}} C^0_{n,p,(n,m)} (h_p - h_n) - \sum_{\substack{q \in \eta_m \\ q \neq n}} C^0_{m,q,(n,m)} (h_q - h_m) \right]. \end{aligned} \tag{45}$$

If h_m is the upstream head, the derivative of equation 31 with respect to h_m can be developed using the approach used to develop equation 45 and results in

$$\begin{aligned} \frac{\partial Q_{n,m}}{\partial h_m} &= C_{n,m,(n,m)} + \sum_{\substack{q \in \eta_m \\ q \neq n}} C_{m,q,(n,m)} \\ &+ \frac{d{S_{F_m}}^*}{dh_m} \left[C^0_{n,m,(n,m)} (h_m - h_n) + \sum_{\substack{p \in \eta_n \\ p \neq m}} C^0_{n,p,(n,m)} (h_p - h_n) - \sum_{\substack{q \in \eta_m \\ q \neq n}} C^0_{m,q,(n,m)} (h_q - h_m) \right]. \end{aligned} \tag{46}$$

For the upstream weighted formulation, the derivatives of saturation with respect to h_n and h_m simplify to

$$\frac{\partial S^*_{Fn}}{\partial h_n} = \begin{cases} \frac{\partial S^*_{Fn}}{\partial h_n} & \text{if } n \text{ is upstream} \\ 0 & \text{if } m \text{ is upstream} \end{cases} \tag{47}$$

and

$$\frac{\partial S^*_{Fm}}{\partial h_m} = \begin{cases} \frac{\partial S^*_{Fm}}{\partial h_m} & \text{if } m \text{ is upstream} \\ 0 & \text{if } n \text{ is upstream} \end{cases} \tag{48}$$

The first two terms on the right-hand side of equations 45 and 46 are already included in the upstream diagonal and appropriate off-diagonal elements of the coefficient matrix during assembly of the conductance-based formulation. The Newton-Raphson formulation is subsequently added as a correction in which the upstream diagonals are augmented with the third terms on the right-hand sides of equations 45 and 46). The products of the third terms on the right-hand sides of equations 45 and 46 and the current, corresponding upstream heads are added to the right-hand side.

Correction Applied by the Horizontal Flow Barrier Package

The Horizontal Flow Barrier (HFB) Package (Hsieh and Freckleton, 1993; Langevin and others, 2017) allows an additional resistance to flow to be placed at a vertical interface between two cells. When the HFB Package is used with the XT3D option, a correction to the flow expression, equation 31, is needed to account for the additional resistance.

Equation 31 was derived under the assumption that the primary interface provides no additional resistance to flow, so that the interfacial head on the cell n side of the interface, $h^*_{n,m}$, is identical to the interfacial head on the cell m side of the interface, $h^*_{m,n}$. However, when a horizontal flow barrier is present, $h^*_{n,m}$ and $h^*_{m,n}$ represent heads on opposite sides of the barrier and, therefore, can differ. In that case, flow across the barrier into cell n from cell m is given by

$$Q^{HFB}_{n,m} = C^{HFB}_{n,m}(h^*_{m,n} - h^*_{n,m}), \tag{49}$$

where $C^{HFB}_{n,m}$ is the conductance of the horizontal flow barrier at interface (n, m). Noting that continuity of flow demands that $Q^{HFB}_{n,m} = Q_{n,m}$, equation 49 can be rearranged to give

$$h^*_{n,m} - h^*_{m,n} = -\frac{Q_{n,m}}{C^{HFB}_{n,m}}. \tag{50}$$

Then, multiplication of equation 26 by $\hat{a}_{m,n}$ and equation 28 by $\hat{a}_{n,m}$; subtraction of the two resulting equations; elimination of $Q_{m,n}$ and $h^*_{n,m} - h^*_{m,n}$ using equations 29 and 50, respectively; and solution for $Q_{n,m}$ gives the XT3D flow expression corrected for the presence of a horizontal flow barrier at the primary interface:

$$\begin{aligned} Q_{n,m} = \; & C_{n,m,(n,m)}\,(h_m - h_n) + \sum_{\substack{p \in \eta_n \\ p \neq m}} C_{n,p,(n,m)}\,(h_p - h_n) - \sum_{\substack{q \in \eta_m \\ q \neq n}} C_{m,q,(n,m)}\,(h_q - h_m) \\ & + C^{HFB}_{n,m,(n,m)}\,(h_m - h_n) + \sum_{\substack{p \in \eta_n \\ p \neq m}} C^{HFB}_{n,p,(n,m)}\,(h_p - h_n) - \sum_{\substack{q \in \eta_m \\ q \neq n}} C^{HFB}_{m,q,(n,m)}\,(h_q - h_m)\,, \end{aligned} \tag{51}$$

where the conductance-like coefficients on the first line are defined as before by equation 32, and the second line represents the HFB correction, in which

$$
\begin{aligned}
C^{HFB}_{n,m,(n,m)} &= -\frac{C^2_{n,m,(n,m)}}{C_{n,m,(n,m)} + C^{HFB}_{n,m}} \\
C^{HFB}_{n,p,(n,m)} &= -\frac{C_{n,p,(n,m)} C_{n,m,(n,m)}}{C_{n,m,(n,m)} + C^{HFB}_{n,m}} \\
C^{HFB}_{m,q,(n,m)} &= -\frac{C_{m,q,(n,m)} C_{n,m,(n,m)}}{C_{n,m,(n,m)} + C^{HFB}_{n,m}}.
\end{aligned}
\tag{52}
$$

For an impermeable barrier, $C^{HFB}_{n,m} = 0$, and substitution of equation 52 into equation 51 results in $Q^{HFB}_{n,m} = 0$. In the absence of a barrier, $C^{HFB}_{n,m} \rightarrow \infty$, the HFB correction terms vanish, and equation 51 reduces to the standard form of the XT3D flow expression, equation 31.

In the MODFLOW 6 code, the matrix form of the CVFD equation, equation 41, is first formulated using the standard XT3D flow expression, equation 31. Coefficients from the HFB correction terms in equation 51 are incorporated into the coefficient matrix, $\mathbf{A}$, in a subsequent step.

Features of the XT3D Option

By default, the XT3D option uses the formulation of the CVFD equation shown in equation 36, which incorporates all of the terms involving "C" coefficients into the coefficient matrix, $\mathbf{A}$, in equation 41; that is, into the "left-hand side" of the matrix equation. When the XT3D Right-Hand Side ("RHS") suboption is active, the XT3D option uses the formulation shown in equation 39, which incorporates some of the terms involving "C" coefficients into the vector $\mathbf{q}$ in equation 41; that is, into the "right-hand side" of the matrix equation.

For many applications, there may be a need to suppress unintended or undesired effects of the three-dimensional geometry of a grid. For example, it may be desirable to suppress certain effects of variations in cell elevation on a model that is intended to simulate two-dimensional, areal groundwater flow. Specifically, when no information is provided by the user on the rotation of the hydraulic conductivity tensor out of the (x, y) plane,

- connections that are not user-designated as vertical are assumed to be strictly horizontal; that is, to have no z component to their orientation, and
- connection lengths are based on horizontal distances.

Applicability and Limitations of the XT3D Option

The XT3D option is applicable to both regular and irregular model grids, whether the conductivity tensor is isotropic or anisotropic. Figure 3 summarizes the conditions under which the standard conductance-based formulation used by the NPF Package of MODFLOW 6 can and cannot provide an accurate representation of flows between cells in the sense of accounting for geometric irregularities and the tensorial nature of Darcy's Law (eq. 1). The "CVFD requirements" are discussed in detail in the GWF Model documentation (Langevin and others, 2017) and are summarized therein as follows:

> "For accurate solutions, the standard CVFD formulation requires that a line drawn between the centers of two connected cells should intersect the shared face at a right angle ... . Furthermore, the intersection point should coincide with an appropriate mean position on the shared face (Narasimhan and Witherspoon, 1976). ... Although this CVFD requirement is met for a simple grid of regular polygons, equilateral triangles, and rectangles, it is violated for nested grids and may be violated for grids with nonregular polygon-shaped cells. ... The smaller the deviation from this CVFD requirement, the smaller the loss of accuracy in the groundwater flow solution. In addition, the errors generally decrease as resolution increases, but they are difficult to quantify."

In cases in which the conductance-based formulation cannot compute flows accurately, the Ghost-Node Connection (GNC) Package can be used to improve accuracy, or the XT3D option can be activated. The GNC Package requires the user to specify points, called "ghost nodes," at which MODFLOW 6 interpolates computed heads to aid in the calculation of more accurate head-gradient estimates. Use of the GNC Package typically requires judgment and additional preprocessing effort to locate and specify appropriate ghost nodes. The XT3D option works with the existing model grid, but it tends to be more computationally intensive than using the standard conductance-based formulation with or without ghost nodes. Figure 4 shows the extended, 25-point stencil used by the XT3D formulation on a regular grid, with cells in the 7-point stencil used by the standard conductance-based formulation shaded gray. Before deciding whether to use the GNC Package or XT3D option for production runs, the user should consider whether the conductance-based formulation alone can provide acceptable accuracy for the particular problem being solved. Trial runs that compare solution accuracy and run times for different formulations can be helpful in this regard. Note that the XT3D option and the GNC Package should not be used simultaneously.

When the head gradient is uniform in the vicinity of a cell interface and its neighboring connections, the XT3D estimate of flow across the interface is exact. When the head gradient is nonuniform, as is typically the case in practice, and anisotropy of the hydraulic conductivity tensor is not aligned with the model-coordinate axes, XT3D handles the gradient nonuniformity by weighted averaging of gradient-component information, as described in the section "Construction of Head-Gradient Vector Expressions on Each Side of the Primary Interface." Such averaging is conceptually similar to the averaging done in standard finite differencing on a rectangular grid (see appendix B). If accuracy is a concern when simulating flow with anisotropy that is not aligned with the model coordinates and driven by substantially nonuniform gradients, such as the gradients associated with strongly diverging or converging flow, grid refinement can be used to estimate the discretization error.

For vertical connections, the XT3D method does not correct for partial dewatering. In that regard, its behavior is similar to the default behavior of MODFLOW 6 for calculating vertical conductances.

Numerical simulations of highly anisotropic flow based on CVFD and finite-element discretizations can exhibit "spurious oscillations" in the solution (Edwards and Zheng, 2010; Pal and Edwards, 2011). Although it can be difficult to distinguish spurious oscillations from legitimate variations in hydraulic head in complex flow systems, solutions calculated using XT3D for highly anisotropic systems should be evaluated critically for evidence of unrealistic patterns in hydraulic head or flow. For example, in a steady-state groundwater flow problem, the head solution should not exhibit a local maximum or minimum within the interior of the model domain unless there is a corresponding source or sink of water at that location.

Example Problems

Three example problems are presented to demonstrate the use of the XT3D option to simulate groundwater flow on irregular grids and through 3D porous media with anisotropic hydraulic conductivity.

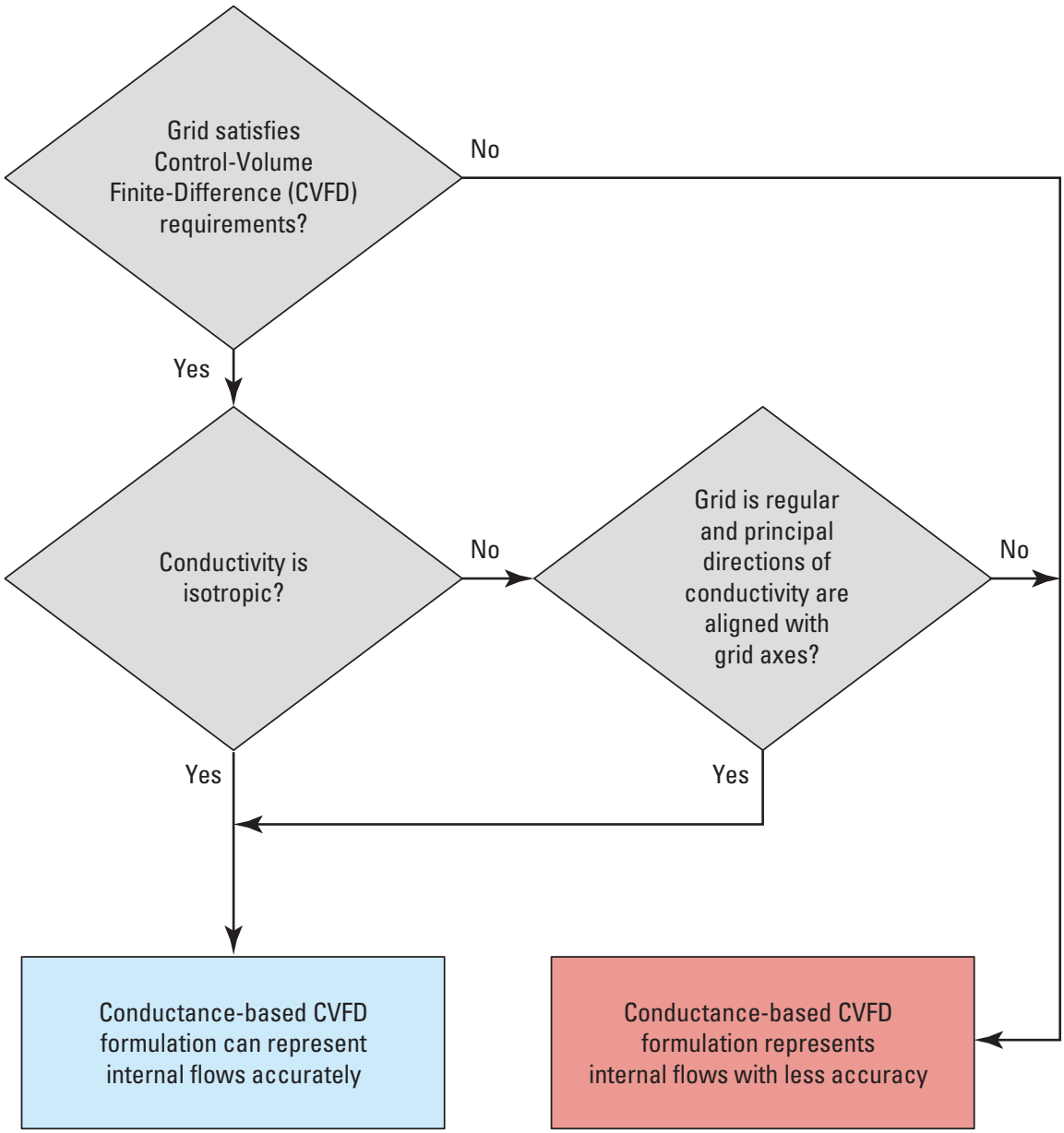

Figure 3. Flowchart showing considerations that affect the accuracy of the conductance-based control-volume finite-difference (CVFD) equation.

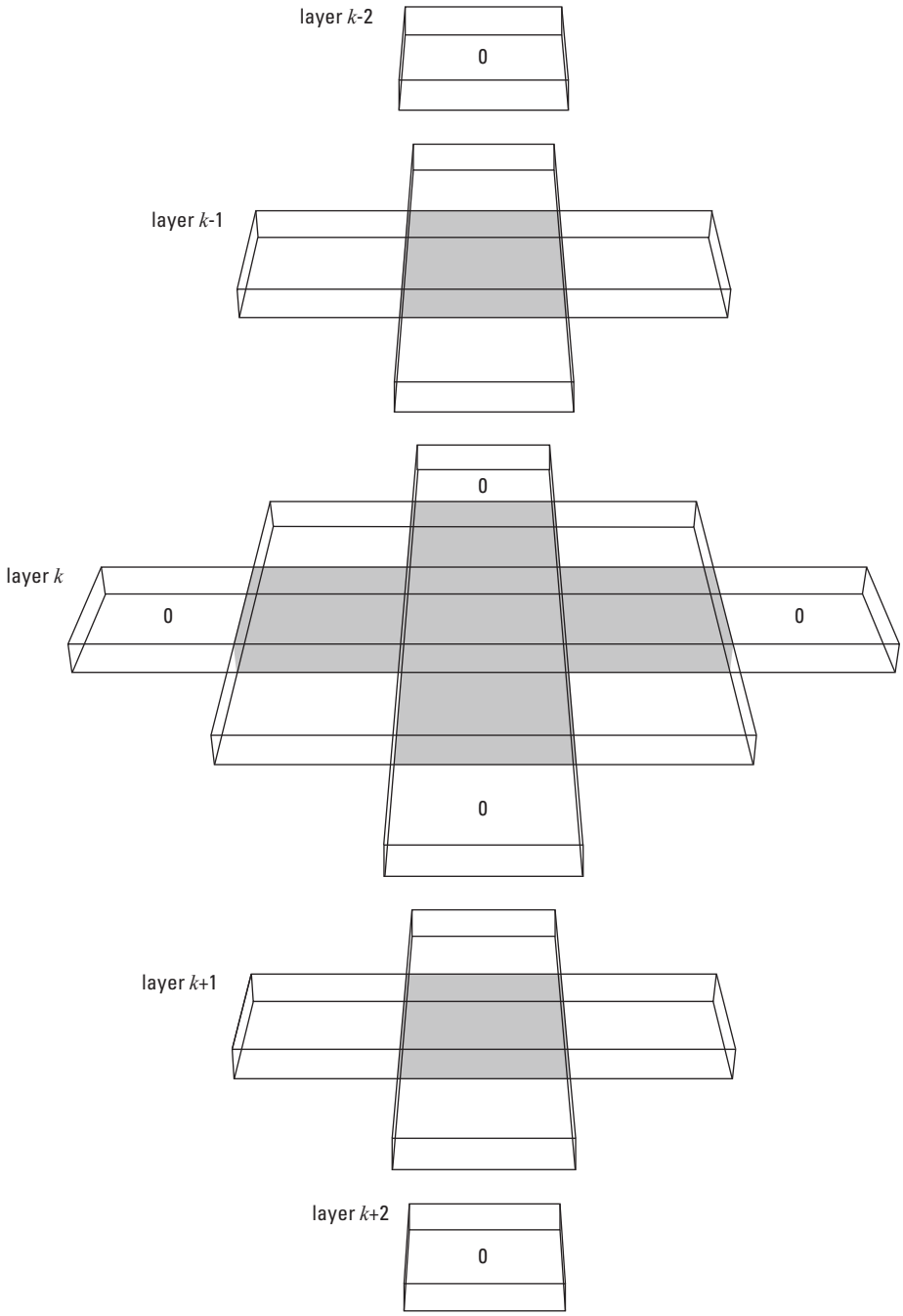

Figure 4. Diagram showing cells in the 25-point stencil used by the XT3D formulation on a regular grid. Cells in the seven-point stencil used by the standard conductance-based formulation on a regular grid are shaded gray. The six cells marked with "0" receive zero weight in the XT3D calculations because their connections with neighbors in the stencil are parallel to primary connections of the central cell, thereby reducing the effective stencil to 19 points on a regular grid.

Example 1: 2D Irregular Grid

This example demonstrates the application of the XT3D option to a two-dimensional (2D) grid (fig. 5) that consists of an irregular, triangular grid nested within a coarser, regular grid. The grid does not satisfy the standard CVFD requirements because, as a rule, the straight-line connection between the centers of two adjacent triangular cells, or between the center of a square cell and the center of an adjacent triangular cell, does not intersect the corresponding cell interface at a right angle. In this case, use of the XT3D option is expected to improve solution accuracy compared to the standard conductance-based formulation used by the NPF Package.

The model domain is 700 meters (m) by 700 m horizontally and 10 m thick. It is discretized into a single layer of cells using the Discretization by Vertices (DISV) Package of the GWF Model (Langevin and others, 2017). The outer portion of the domain is discretized horizontally into 100-m by 100-m square cells. A 300-m by 300-m square at the center of the domain is discretized horizontally into triangular cells approximately 30 m on a side. A constant head of 0.65 m is specified at nodes in the leftmost column of cells, and a constant head of 0.05 m is specified at nodes in the rightmost column of cells. The cells are confined, and the hydraulic conductivity is isotropic and set to a value of 1 meter per day (m/d). The numerical problem was solved using the BiCGSTAB linear accelerator (Saad, 2003) with the convergence tolerances for head, `OUTER_HCLOSE` and `INNER_HCLOSE`, both set to 10^{-8} m, and `INNER_RCLOSE` set to 10^{-2} cubic meters per day (m^3/d).

The exact solution to this problem is a uniform, left-to-right head gradient of 0.001 and a total flow through the domain of 7 m^3/d. Figure 6 compares the errors in the heads (exact solution minus simulated solution) for the standard conductance-based formulation and the XT3D option. The largest error in head obtained using the standard conductance-based formulation was -0.012 m, or -2.0% of the difference between the maximum and minimum heads in the problem. The largest error in head obtained using the XT3D option was -3.8×10^{-10} m, which is less than the convergence tolerances for head. The flow through the model domain (reported to four decimal places in the volume budget in the listing file) simulated using the standard conductance-based formulation was 7.0919 (-1.3% error). The flow simulated using the XT3D option was 7.0000 m^3/d.

Example 2: 3D Anisotropic Conductivity

This example is an extension of example 1 that demonstrates the ability of the XT3D option to accurately simulate 3D anisotropic flow. The single-layer grid used in example 1 is extended to five layers, each of which is 10 m thick and is discretized horizontally as in example 1. All cells adjacent to the outer boundary of the model domain are constant-head cells with heads that correspond to the 3D extension of the uniform, left-to-right gradient of 0.001 simulated in example 1. The XT3D option is active, with hydraulic conductivities set to achieve 10:5:1 anisotropy rotated 45° counterclockwise from the x axis and 30° upward from the horizontal plane: $K11 = 1$ m/d, $K22 = 0.5$ m/d, $K33 = 0.1$ m/d, $ANGLE1 = 45°$, and $ANGLE2 = 30°$. All other input for this example remains the same as in example 1.

Within each layer, the exact head solution is the same as for the single-layer problem in example 1. The maximum error in simulated head was 3.3×10^{-10} m, which is less than the convergence tolerances for head. Due to anisotropy, the groundwater flux in this example differs in magnitude and direction from the flow in example 1. The exact solution for total flow through the active part of the domain (which excludes constant-head cells) is 80.5169 m^3/d, rounded to four decimal places. The total simulated flow through the active part of the domain (reported to four decimal places in the volume budget in the listing file) was 80.5169 m^3/d.

Example 3: Groundwater Whirls

Using steady-state groundwater flow simulations, Hemker and others (2004) have shown that "spiraling flow lines occur in layered aquifers that have different anisotropic horizontal hydraulic conductivities in adja-

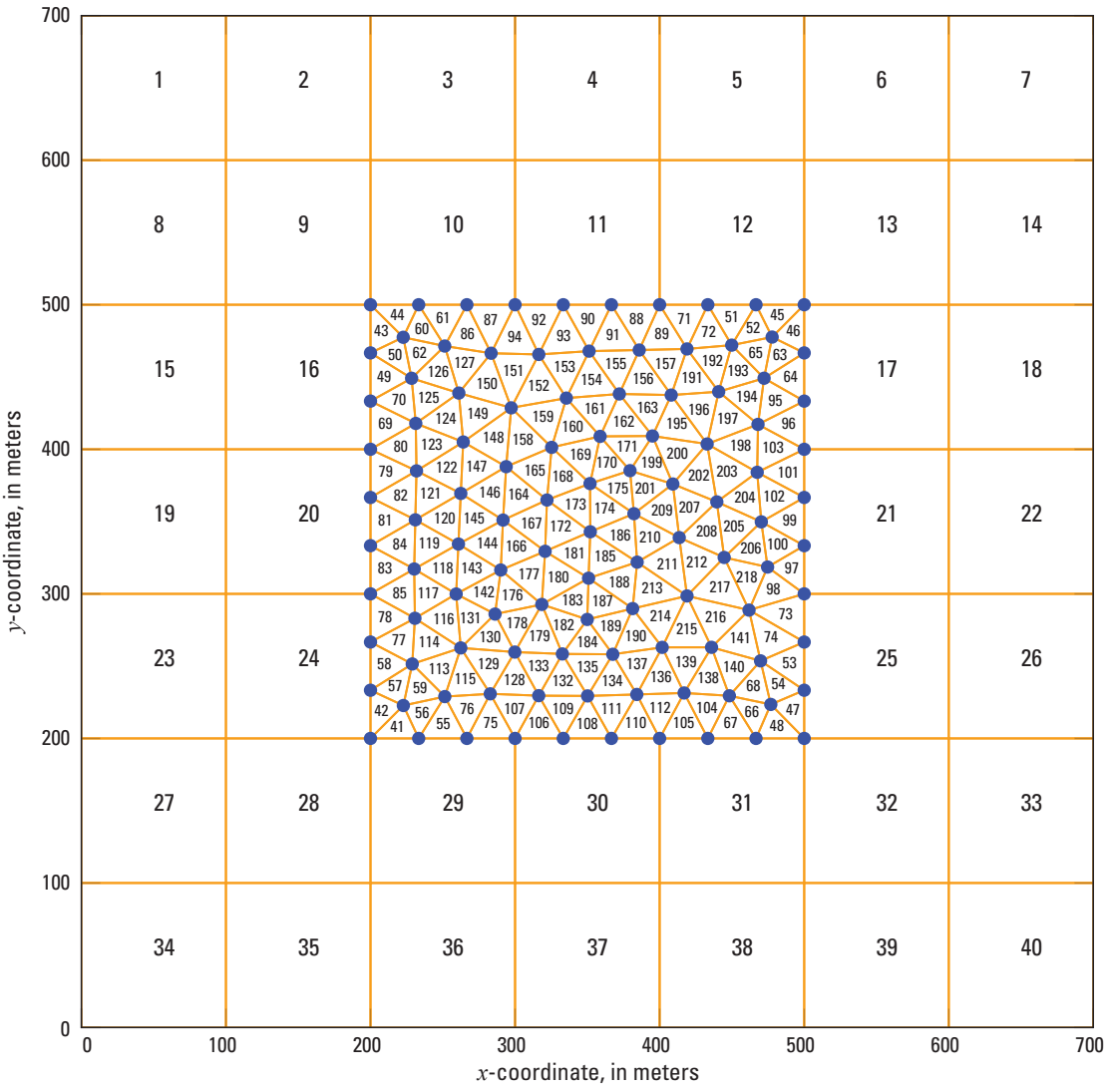

Figure 5. Diagram showing the two-dimensional (2D) irregular grid used in example 1, which features a triangular grid nested within a regular grid, does not satisfy the standard CVFD requirements. The grid in this diagram is defined using the Discretization by Vertices (DISV) Package of the GWF Model of MODFLOW 6 (Langevin and others, 2017). Numbers inside cells show the cell numbering.

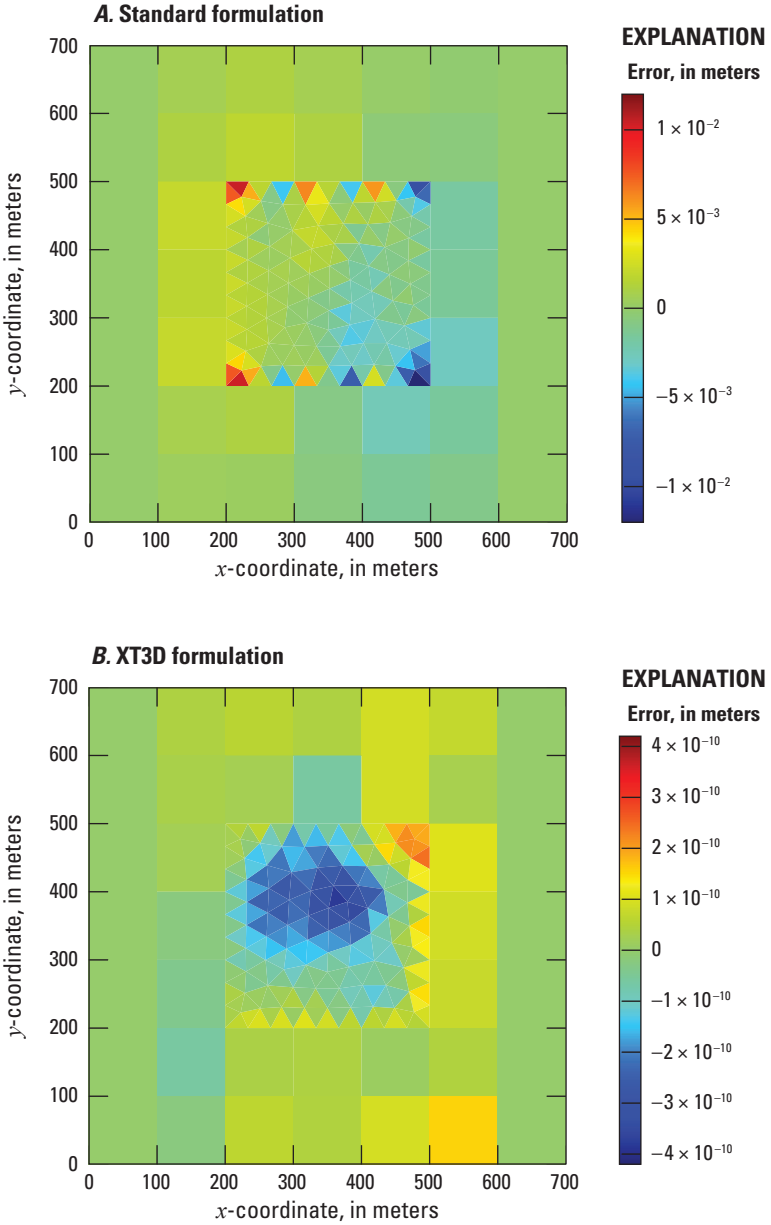

Figure 6. Plot showing errors in simulated heads in example 1: *A*, using the standard conductance-based formulation, and *B*, using the XT3D option. Note the different color scales in *A* and *B*.

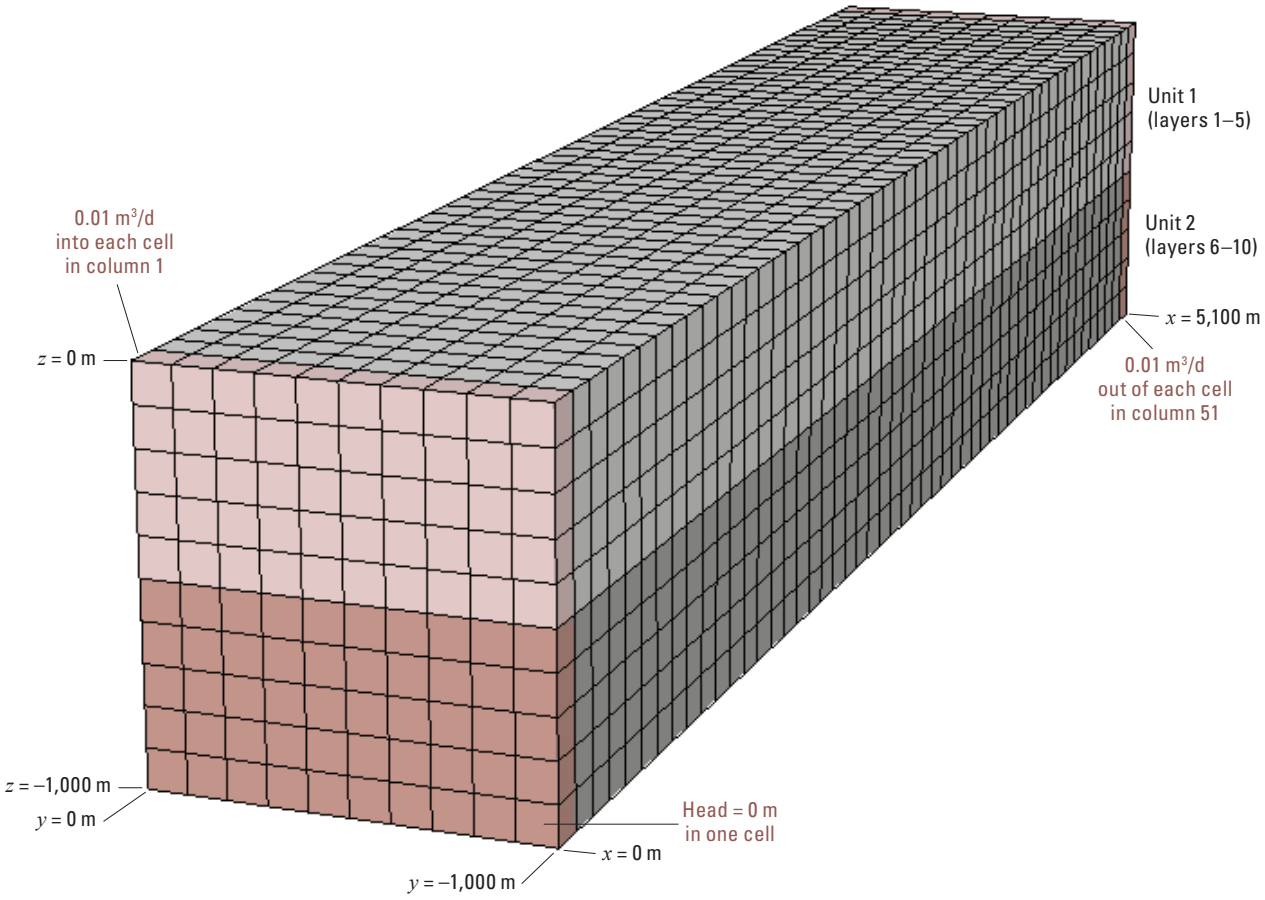

Figure 7. Diagram showing the model domain for example 3, which is a three-dimensional box with two hydrogeologic units (light and dark shading). Groundwater is injected into one end of the box (column 1, pink shading) at a rate of 0.01 cubic meters per day (m^3/d) into each cell and is removed from the opposite end of the box (column 51, pink shading) at a rate of 0.01 m^3/d from each cell. A constant head of 0 meters (m) is set in one of the corner cells to anchor the steady-state head distribution.

cent layers." They refer to such spiraling flow lines as "groundwater whirls." This example demonstrates the use of the XT3D option to implement anisotropy that induces groundwater whirls in a highly idealized two-aquifer system. Results are presented for three sets of hydraulic conductivity parameters: two that involve rotation of the principal directions of conductivity only within the horizontal plane, and one that includes rotation out of the horizontal plane. Flow lines are visualized by particle tracking using MODPATH (Pollock, 2016).

The model domain (fig. 7) is a box that is 5,100 m by 1,000 m horizontally and 1,000 m thick, discretized into a regular grid of 10 rows, 51 columns, and 10 layers. The top five model layers form the top aquifer, and the bottom five model layers form the bottom aquifer. All cells are confined. Aquifer properties are homogeneous within each aquifer but differ between the aquifers. Groundwater recharges one end of the box at a total rate of 1 m^3/d, distributed equally among 100 cells, and is removed from the opposite end of the box at the same rate, also distributed equally among 100 cells. The numerical problem was solved using the BiCGSTAB linear accelerator (Saad, 2003) with the convergence tolerances for head, `OUTER_HCLOSE` and `INNER_HCLOSE`, both set to 10^{-8} m, and `INNER_RCLOSE` set to 10^{-2} m^3/d.

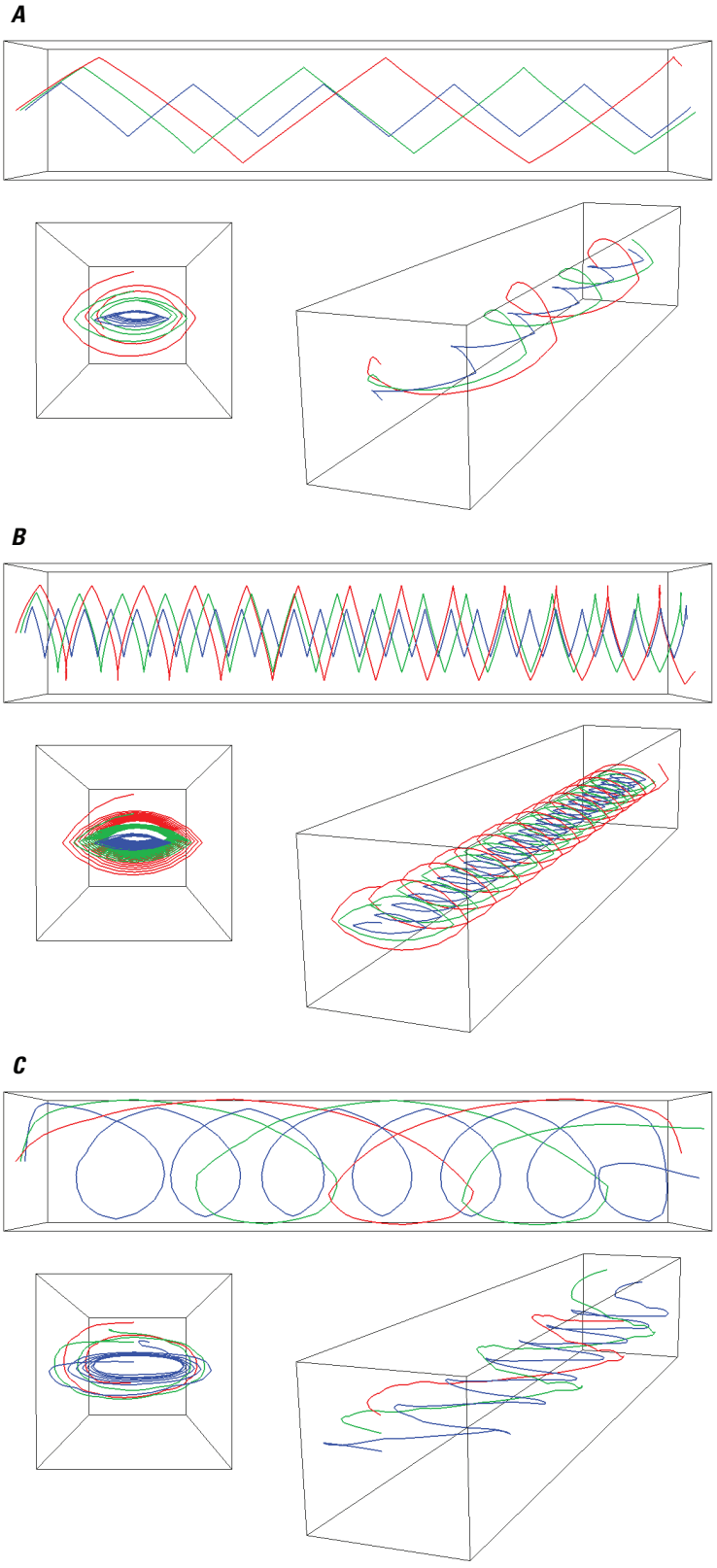

Figure 8. Plots that show top, end, and oblique views of groundwater whirls generated in the three cases of anisotropic conductivity considered in example 3. In cases *A* and *B*, rotation of the principal directions of conductivity is only within the horizontal plane. Case *C* involves rotations of the principal directions of conductivity both within and out of the horizontal plane. Red, green, and blue flow lines are based on tracks of three different particles computed using MODPATH (Pollock, 2016).

The first case features 10:1 horizontal anisotropy ($K11 = K33 = 1$ m/d, $K22 = 0.1$ m/d) rotated 45° counterclockwise from the x axis ($ANGLE1 = 45°$, $ANGLE2 = ANGLE3 = 0°$) in the top aquifer and 45° clockwise from the x axis ($ANGLE1 = -45°$, $ANGLE2 = ANGLE3 = 0°$) in the bottom aquifer. Figure 8*A* shows the resulting swirling flow lines, or groundwater whirls.

The second case is the same as the first, except that the horizontal anisotropy ratio is increased to 1000:1 ($K22 = 0.001$ m/d) and the rotation from the x axis is increased to 75° counterclockwise ($ANGLE1 = 75°$) in the top aquifer and 75° clockwise ($ANGLE1 = -75°$) in bottom aquifer. Figure 8*B* shows the resulting groundwater whirls, which exhibit more revolutions over the length of the model domain than in the first case.

The third and final case is the same as the second, except for the addition of 75° rotations of the principal axes of conductivity about the $K11$ axis in the top and bottom aquifers ($ANGLE3 = 75°$ and $ANGLE3 = -75°$, respectively). Figure 8*C* shows the resulting groundwater whirls, which, interestingly, reverse direction as they progress from one end of the box to the other.

References Cited

Anderman, E.R., Kipp, K.L., Hill, M.C., Valstar, Johan, and Neupauer, R.M., 2002, MODFLOW-2000, the U.S. Geological Survey modular ground-water model—Documentation of the Model-Layer Variable-Direction Horizontal Anisotropy (LVDA) capability of the Hydrogeologic-Unit Flow (HUF) Package: U.S. Geological Survey Open-File Report 02–409, 60 p., accessed June 27, 2017, at https://pubs.er.usgs.gov/publication/ofr02409.

Diskin, Boris, and Thomas, J.L., 2008, Accuracy of gradient reconstruction on grids with high aspect ratio: National Institute of Aerospace Report No. 2008–12, 25 p.

Diskin, Boris, and Thomas, J.L., 2011, Comparison of node-centered and cell-centered unstructured finite-volume discretizations—Inviscid fluxes: American Institute of Aeronautics and Astronautics Journal, v. 49, no. 4, p. 836–854, accessed June 27, 2017, at https://doi.org/10.2514/1.J050897.

Edwards, M.G., and Zheng, Hongwen, 2010, Double-families of quasi-positive Darcy-flux approximations with highly anisotropic tensors on structured and unstructured grids: Journal of Computational Physics, v. 229, no. 3, p. 594–625, accessed June 27, 2017, at https://doi.org/10.1016/j.jcp.2009.09.037.

Freeze, R.A., and Cherry, J.A., 1979, Groundwater: Englewood Cliffs, N.J., Prentice-Hall, 604 p.

Hemker, Kick, van den Berg, Elmer, and Bakker, Mark, 2004, Ground water whirls: Ground Water, v. 42, no. 2, p. 234–242, accessed June 27, 2017, at https://doi.org/10.1111/j.1745-6584.2004.tb02670.x.

Hsieh, P.A., and Freckleton, J.R., 1993, Documentation of a computer program to simulate horizontal-flow barriers using the U.S. Geological Survey's modular three-dimensional finite-difference ground-water flow model: U.S. Geological Survey Open-File Report 92–477, 32 p., accessed June 27, 2017, at https://pubs.er.usgs.gov/publication/ofr92477.

Langevin, C.D., Hughes, J.D., Provost, A.M., Banta, E.R., Niswonger, R.G., and Panday, Sorab, 2017, Documentation for the MODFLOW 6 Groundwater Flow (GWF) Model: U.S. Geological Survey Techniques and Methods, book 6, chap. A55, 197 p., accessed August 4, 2017, at https://doi.org/10.3133/tm6A55.

Mavriplis, D.J., 2003, Revisiting the least-squares procedure for gradient reconstruction on unstructured meshes: 16th American Institute of Aeronautics and Astronautics Computational Fluid Dynamics Conference, Paper 2003-3986, 13 p., accessed June 27, 2017, at https://doi.org/10.2514/6.2003-3986.

Narasimhan, T.N., and Witherspoon, P.A., 1976, An integrated finite difference method for analyzing fluid flow in porous media: Water Resources Research, v. 12, no. 1, p. 57–64, accessed June 27, 2017, at https://doi.org/10.1029/WR012i001p00057.

Pal, Mayur, and Edwards, M.G., 2011, Non-linear flux-splitting schemes with imposed discrete maximum principle for elliptic equations with highly anisotropic coefficients: International Journal for Numerical Methods in Fluids, v. 66, no. 3, p. 299–323, accessed June 27, 2017, at https://doi.org/10.1002/fld.2258.

Panday, Sorab, Langevin, C.D., Niswonger, R.G., Ibaraki, Motomu, and Hughes, J.D., 2013, MODFLOW-USG version 1—An unstructured grid version of MODFLOW for simulating groundwater flow and tightly coupled processes using a control volume finite-difference formulation: U.S. Geological Survey Techniques and Methods, book 6, chap. A45, 66 p., accessed June 27, 2017, at https://pubs.usgs.gov/tm/06/a45/.

Pollock, D.W., 2016, User guide for MODPATH Version 7—A particle-tracking model for MODFLOW: U.S. Geological Survey Open-File Report 2016–1086, 35 p., accessed June 27, 2017, at https://doi.org/10.3133/ofr20161086.

Rushton, K.R., and Redshaw, S.C., 1979, Seepage and groundwater flow: numerical analysis by analogue and digital methods: New York, John Wiley and Sons, 339 p.

Saad, Yousef, 2003, Iterative methods for sparse linear systems: Philadelphia, Penn., Society for Industrial and Applied Mathematics, 528 p., accessed June 27, 2017, at https://doi.org/10.1137/1.9780898718003.

Zheng, Chunmiao, and Wang, P.P., 1999, MT3DMS—A modular three-dimensional multi-species transport model for simulation of advection, dispersion and chemical reactions of contaminants in groundwater systems; Documentation and user's guide: Contract report SERDP–99–1: Vicksburg, Miss., U.S. Army Engineer Research and Development Center, 169 p.

Appendix A. List of Symbols

The following is a list of symbols used in this report.

Table A–1. List of symbols used in this report.

Symbol	Description	Dimension
$\in$	mathematical symbol that denotes membership in a set	-
$\sum_{m \in \eta_n}$	summation over cells connected to cell n	-
$\sum_{\substack{p \in \eta_n \\ p \neq m}}$	summation over cells connected to cell n, excluding cell m	-
α^u	coefficient defined in equation 15 (for various u)	-
$\beta^u_{n,p}$	coefficient defined in equation 15 (for various u)	-
$\boldsymbol{\gamma}$	hydraulic-head gradient ($\equiv \boldsymbol{\nabla} h$)	-
$\boldsymbol{\gamma}_{n,p}$	hydraulic-head gradient vector at connection (n,p)	-
$\gamma^u_{n,p}$	u-coordinate component of $\boldsymbol{\gamma}_{n,p}$ (for various u)	-
∂	partial differential operator	-
$\boldsymbol{\nabla}$	gradient operator	L^{-1}
η_n	list of cells connected to cell n	-
$\varphi^u_{n,p}$	weight for u-component gradient estimate from connection (n,p) (for various u)	-
$\boldsymbol{\sigma}$	vector defined in equation 22	LT^{-1}
$\omega^v_{n,p}$	coefficient defined in equation 18 (for various v)	-
$a_{n,m}$	coefficient defined in equation 21	LT^{-1}
$\hat{a}_{n,m}$	coefficient defined in equation 27	L^2T^{-1}
$A_{n,m}$	area of the primary interface, (n,m), associated with cell n	L^2
$A_{m,n}$	area of the primary interface, (n,m), associated with cell m	L^2
$b_{n,p,(n,m)}$	coefficient defined in equation 21	LT^{-1}
$\hat{b}_{n,p,(n,m)}$	coefficient defined in equation 27	L^2T^{-1}
$A^{u,v}$	coefficient defined in equation 16 (for various u, v)	-
$B^v_{n,p}$	coefficient defined in equation 16 (for various v)	-
$\mathbf{c}$	unit connection-orientation vector	-
$\mathbf{c}_{n,p}$	unit connection-orientation vector for connection (n,p)	-
$\mathbf{c}^u_{n,p}$	u-coordinate component of $\mathbf{c}_{n,p}$ (for various u)	-
$C_{n,m}$	hydraulic conductance between cells n and m	L^2T^{-1}
$C^{HFB}_{n,m}$	hydraulic conductance of horizontal flow barrier at interface (n,m)	L^2T^{-1}
$C_{n,m,(n,m)}$	conductance-like coefficient in the XT3D flow expression, equation 31	L^2T^{-1}
$C_{n,p,(n,m)}$	conductance-like coefficient in the XT3D flow expression, equation 31	L^2T^{-1}
$C_{m,q,(n,m)}$	conductance-like coefficient in the XT3D flow expression, equation 31	L^2T^{-1}
$C^0_{n,m,(n,m)}$	value of $C_{n,m,(n,m)}$ at full saturation	L^2T^{-1}
$C^0_{n,p,(n,m)}$	value of $C_{n,p,(n,m)}$ at full saturation	L^2T^{-1}
$C^0_{m,q,(n,m)}$	value of $C_{m,q,(n,m)}$ at full saturation	L^2T^{-1}
C_1, C_2, C_3	cosines of coordinate-rotation angles, defined in equation 24	-
$D_{n,p}$	distance between the midpoint of connection (n,p) and point on the primary interface	L
h	hydraulic head	L
$h^*_{n,m}$	interfacial head for cell n at the primary interface, (n,m)	L
$HCOF_n$	head coefficient in the XT3D CVFD equation, defined in equation 37	L^2T^{-1}
$HOLD_n$	head in cell n at the end of the previous time step	L

Table A–1. List of symbols used in this report.—Continued

Symbol	Description	Dimension
$\mathbf{K}$	hydraulic conductivity tensor	LT^{-1}
K_{xx}	one of three "diagonal" hydraulic conductivities	LT^{-1}
K_{yy}	one of three "diagonal" hydraulic conductivities	LT^{-1}
K_{zz}	one of three "diagonal" hydraulic conductivities	LT^{-1}
K_{xy}	one of three "off-diagonal" hydraulic conductivities	LT^{-1}
K_{xz}	one of three "off-diagonal" hydraulic conductivities	LT^{-1}
K_{yz}	one of three "off-diagonal" hydraulic conductivities	LT^{-1}
l	distance between cell centers on a square grid	L
$l_{n,m}$	distance between centers of cells n and m	L
l_x	distance between centers of cells along the x direction on a uniformly spaced grid	L
l_y	distance between centers of cells along the y direction on a uniformly spaced grid	L
l_z	distance between centers of cells along the z direction on a uniformly spaced grid	L
$L_{n,m}$	distance between center of cell n and its shared face with m	L
m subscript	cell number	-
n subscript	cell number	-
(n, m)	connection between cells n and m	-
$\mathbf{n}_{n,m}$	unit vector normal to the primary interface, (n, m)	-
p subscript	cell number	-
P_n	sum of external-stress coefficients for cell n	L^2T^{-1}
q subscript	cell number	-
$\mathbf{q}$	specific discharge vector	LT^{-1}
$q_{n,m}$	normal flux into cell n at the primary interface, (n, m)	LT^{-1}
Q_n	sum of external-stress coefficients for cell n	L^3T^{-1}
$Q_{n,m}$	volumetric flow rate from cell m into cell n	L^3T^{-1}
$Q_{n,m}^{HFB}$	volumetric flow rate from cell m into cell n across horizontal flow barrier	L^2T^{-1}
Q'_s	source or sink volumetric flux per unit volume	T^{-1}
$\mathbf{R}$	rotation matrix that transforms vectors from (x_1, y_1, z_1) to (x, y, z) coordinates	-
RHS_n	right-hand side of the XT3D CVFD equation, defined in equation 38	L^3T^{-1}
RHS_n^*	modified right-hand side of the XT3D CVFD equation, defined in equation 40	L^3T^{-1}
${S_{F_n}}^*$	smoothed saturated fraction of cell n	-
S_S	specific storage	L^{-1}
SS_n	specific storage of cell n	L^{-1}
S_1, S_2, S_3	sines of coordinate-rotation angles, defined in equation 24	-
t	time	T
t_{old}	time at the end of the previous time step	T
Δv_n^0	thickness of cell n (fully saturated)	L
ΔV_n	volume of cell n	L^3
$\Delta w_{n,m}$	width of the primary interface, (n, m)	L
x	x coordinate in model coordinates	L
$x_{n,p}$	local x coordinate along cell connection (n, p)	L
x_1	local x coordinate along primary connection ($\equiv x_{n,m}$)	L
y	y coordinate in model coordinates	L
$y_{n,p}$	local y coordinate perdendicular to cell connection (n, p)	L

Table A–1. List of symbols used in this report.—Continued

Symbol	Description	Dimension
y_1	local y coordinate along primary connection ($\equiv y_{n,m}$)	L
z	z coordinate in model coordinates	L
$z_{n,p}$	local z coordinate perdendicular to cell connection (n, p)	L
z_1	local z coordinate along primary connection ($\equiv z_{n,m}$)	L

Appendix B. XT3D Calculations on a Rectangular Grid

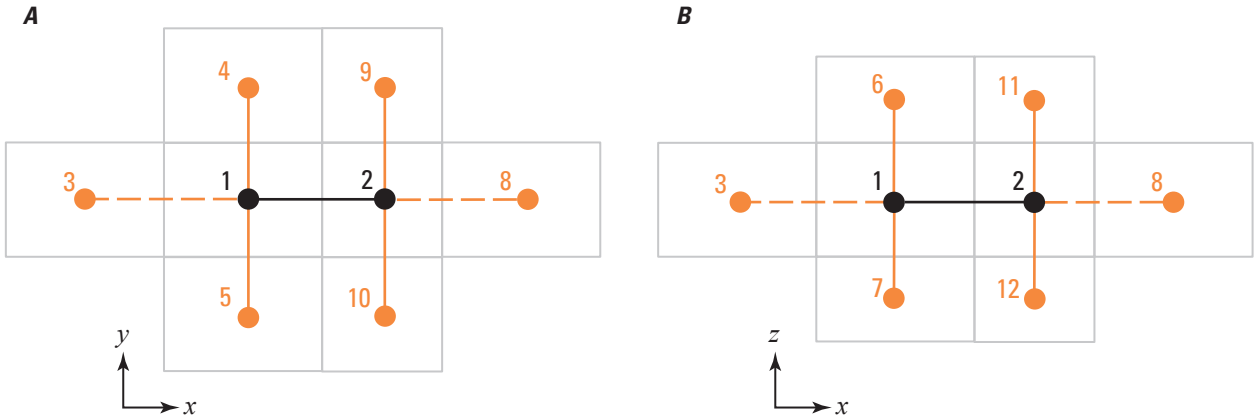

Figure B–1. Illustration of a portion of a rectangular, three-dimensional (3D) grid that includes two cells (cells 1 and 2) and their immediate neighbors. *A*, view projected onto the (x, y) plane, and *B*, view projected onto the (x, z) plane. The primary connection is shown in black. Neighboring connections are shown in orange. Neighboring connections shown using dashed lines receive zero weight in the XT3D head-gradient calculations because they are parallel to the primary connection.

On a rectangular grid, the connections between cells are aligned with the coordinate axes. On the portion of a rectangular grid shown in figure B–1, the components of the connection-orientation vectors are

$$
\begin{aligned}
&c^y_{1,2} = c^y_{1,3} = c^y_{1,6} = c^y_{1,7} = 0 \\
&c^y_{1,4} = 1 \\
&c^y_{1,5} = -1 \\
&c^z_{1,2} = c^z_{1,3} = c^z_{1,4} = c^z_{1,5} = 0 \\
&c^z_{1,6} = 1 \\
&c^z_{1,7} = -1.
\end{aligned}
\tag{B–1}
$$

Substitution of the components in equation B–1 into equation 18 gives

$$
\begin{aligned}
&\omega^y_{1,2} = \omega^y_{1,3} = \omega^y_{1,6} = \omega^y_{1,7} = 0 \\
&\omega^y_{1,4} = \frac{D_{1,5}}{D_{1,4} + D_{1,5}} \\
&\omega^y_{1,5} = \frac{D_{1,4}}{D_{1,4} + D_{1,5}} \\
&\omega^z_{1,2} = \omega^z_{1,3} = \omega^z_{1,4} = \omega^z_{1,5} = 0 \\
&\omega^z_{1,6} = \frac{D_{1,7}}{D_{1,6} + D_{1,7}} \\
&\omega^z_{1,7} = \frac{D_{1,6}}{D_{1,6} + D_{1,7}}.
\end{aligned}
\tag{B–2}
$$

Connection-midpoint distances can be expressed in terms of connection lengths as follows:

$$
\begin{aligned}
D_{1,4} &= \left(L_{1,2}^2 + l_{1,4}^2/4\right)^{1/2} \\
D_{1,5} &= \left(L_{1,2}^2 + l_{1,5}^2/4\right)^{1/2} \\
D_{1,6} &= \left(L_{1,2}^2 + l_{1,6}^2/4\right)^{1/2} \\
D_{1,7} &= \left(L_{1,2}^2 + l_{1,7}^2/4\right)^{1/2} \\
D_{2,9} &= \left(L_{1,2}^2 + l_{1,9}^2/4\right)^{1/2} \\
D_{2,10} &= \left(L_{1,2}^2 + l_{1,10}^2/4\right)^{1/2} \\
D_{2,11} &= \left(L_{1,2}^2 + l_{1,11}^2/4\right)^{1/2} \\
D_{2,12} &= \left(L_{1,2}^2 + l_{1,12}^2/4\right)^{1/2}.
\end{aligned}
\tag{B–3}
$$

Substitution of equations B–1 and B–2 into equation 17 then gives the following weights:

$$
\begin{aligned}
\varphi_{1,2}^y &= \varphi_{1,3}^y = \varphi_{1,6}^y = \varphi_{1,7}^y = 0 \\
\varphi_{1,4}^y &= \frac{D_{1,5}}{D_{1,4} + D_{1,5}} \\
\varphi_{1,5}^y &= \frac{D_{1,4}}{D_{1,4} + D_{1,5}} \\
\varphi_{1,2}^z &= \varphi_{1,3}^z = \varphi_{1,4}^z = \varphi_{1,5}^z = 0 \\
\varphi_{1,6}^z &= \frac{D_{1,7}}{D_{1,6} + D_{1,7}} \\
\varphi_{1,7}^z &= \frac{D_{1,6}}{D_{1,6} + D_{1,7}}.
\end{aligned}
\tag{B–4}
$$

Substitution of equations B–1 and B–4 into equation 16 gives

$$
\begin{aligned}
A^{xy} &= A^{xz} = A^{yz} = A^{zy} = 0 \\
B_{1,2}^y &= B_{1,3}^y = B_{1,6}^y = B_{1,7}^y = 0 \\
B_{1,4}^y &= \frac{D_{1,5}}{D_{1,4} + D_{1,5}} \\
B_{1,5}^y &= \frac{-D_{1,4}}{D_{1,4} + D_{1,5}} \\
B_{1,2}^z &= B_{1,3}^z = B_{1,4}^z = B_{1,5}^z = 0 \\
B_{1,6}^y &= \frac{D_{1,7}}{D_{1,6} + D_{1,7}} \\
B_{1,7}^y &= \frac{-D_{1,6}}{D_{1,6} + D_{1,7}},
\end{aligned}
\tag{B–5}
$$

and substitution of equation B–5 into equation 15 then gives

$$
\begin{aligned}
\alpha^y &= \alpha^z = 0 \\
\beta^y_{1,2} &= \beta^y_{1,3} = \beta^y_{1,6} = \beta^y_{1,7} = 0 \\
\beta^y_{1,4} &= \frac{D_{1,5}}{D_{1,4} + D_{1,5}} \\
\beta^y_{1,5} &= \frac{-D_{1,4}}{D_{1,4} + D_{1,5}} \\
\beta^z_{1,2} &= \beta^z_{1,3} = \beta^z_{1,4} = \beta^z_{1,5} = 0 \\
\beta^y_{1,6} &= \frac{D_{1,7}}{D_{1,6} + D_{1,7}} \\
\beta^y_{1,7} &= \frac{-D_{1,6}}{D_{1,6} + D_{1,7}}.
\end{aligned}
\tag{B–6}
$$

Recognizing that the unit normal vector for the primary interface is

$$
\mathbf{n}_{1,2} = \begin{pmatrix} 1 \\ 0 \\ 0 \end{pmatrix} \tag{B–7}
$$

and that the local coordinates used for the gradient calculations coincide with the model coordinates, so that there is no rotation of local coordinates relative to model coordinates,

$$
\mathbf{R} = \begin{pmatrix} 1 & 0 & 0 \\ 0 & 1 & 0 \\ 0 & 0 & 1 \end{pmatrix}, \tag{B–8}
$$

one can write equation 22 as

$$
\boldsymbol{\sigma} = \begin{pmatrix} K_{xx_1} \\ K_{xy_1} \\ K_{xz_1} \end{pmatrix}, \tag{B–9}
$$

where the subscript "1" indicates that the conductivitites are for cell 1. Substitution of equations B–6 and B–9 into equation 21 gives

$$
\begin{aligned}
a_{1,2} &= K_{xx_1} \\
b^y_{1,2,(1,2)} &= b^y_{1,3,(1,2)} = 0 \\
b^y_{1,4,(1,2)} &= \frac{K_{xy_1} D_{1,5}}{D_{1,4} + D_{1,5}} \\
b^y_{1,5,(1,2)} &= \frac{-K_{xy_1} D_{1,4}}{D_{1,4} + D_{1,5}} \\
b^y_{1,6,(1,2)} &= \frac{K_{xz_1} D_{1,7}}{D_{1,6} + D_{1,7}} \\
b^y_{1,7,(1,2)} &= \frac{-K_{xz_1} D_{1,6}}{D_{1,6} + D_{1,7}}.
\end{aligned}
\tag{B–10}
$$

Using the same interfacial area on both sides of the interface,

$$
A_{2,1} = A_{1,2}, \tag{B–11}
$$

and substituting equation B–10 into equation 27, one obtains

$$
\begin{aligned}
\hat{a}_{1,2} &= \frac{K_{xx_1} A_{1,2}}{L_{1,2}} \\
\hat{b}^y_{1,2,(1,2)} &= \hat{b}^y_{1,3,(1,2)} = 0 \\
\hat{b}^y_{1,4,(1,2)} &= \frac{K_{xy_1} A_{1,2}}{l_{1,4}} \left(\frac{D_{1,5}}{D_{1,4} + D_{1,5}} \right) \\
\hat{b}^y_{1,5,(1,2)} &= \frac{K_{xy_1} A_{1,2}}{l_{1,5}} \left(\frac{-D_{1,4}}{D_{1,4} + D_{1,5}} \right) \\
\hat{b}^y_{1,6,(1,2)} &= \frac{K_{xz_1} A_{1,2}}{l_{1,6}} \left(\frac{D_{1,7}}{D_{1,6} + D_{6,4}} \right) \\
\hat{b}^y_{1,7,(1,2)} &= \frac{K_{xz_1} A_{1,2}}{l_{1,7}} \left(\frac{-D_{1,6}}{D_{1,6} + D_{1,7}} \right).
\end{aligned}
\tag{B–12}
$$

Substitution of equation B–12 into equation 26 and rearrangement then gives the expression for the normal flux from cell 2 into cell 1:

$$
\begin{aligned}
q_{1,2} &= \frac{Q_{1,2}}{A_{1,2}} \\
&= K_{xx_1} \left(\frac{h^*_{1,2} - h_1}{L_{1,2}} \right) + K_{xy_1} \left[\frac{D_{1,5}}{D_{1,4} + D_{1,5}} \left(\frac{h_4 - h_1}{l_{1,4}} \right) + \frac{D_{1,4}}{D_{1,4} + D_{1,5}} \left(\frac{h_1 - h_5}{l_{1,5}} \right) \right] \\
&\quad + K_{xz_1} \left[\frac{D_{1,7}}{D_{1,6} + D_{1,7}} \left(\frac{h_6 - h_1}{l_{1,6}} \right) + \frac{D_{1,6}}{D_{1,6} + D_{1,7}} \left(\frac{h_1 - h_7}{l_{1,7}} \right) \right].
\end{aligned}
\tag{B–13}
$$

An analogous series of calculations for cell 2, using the same interfacial head,

$$h^*_{2,1} = h^*_{1,2}, \tag{B–14}$$

yields an analogous expression for the normal flux from cell 1 into cell 2:

$$\begin{aligned} q_{2,1} &= \frac{Q_{2,1}}{A_{2,1}} \\ &= K_{xx_2}\left(\frac{h^*_{2,1}-h_2}{L_{2,1}}\right) + K_{xy_2}\left[\frac{D_{2,10}}{D_{2,9}+D_{2,10}}\left(\frac{h_9-h_2}{l_{1,9}}\right) + \frac{D_{2,9}}{D_{2,9}+D_{2,10}}\left(\frac{h_2-h_{10}}{l_{2,10}}\right)\right] \\ &\quad + K_{xz_2}\left[\frac{D_{2,12}}{D_{2,11}+D_{2,12}}\left(\frac{h_{11}-h_2}{l_{2,11}}\right) + \frac{D_{2,11}}{D_{2,11}+D_{2,12}}\left(\frac{h_2-h_{12}}{l_{2,12}}\right)\right]. \end{aligned} \tag{B–15}$$

Continutity of flow requires that the fluxes given by equations B–13 and B–15 must be equal in magnitude and opposite in sign:

$$q_{1,2} = -q_{2,1}. \tag{B–16}$$

Substitution of equations B–13 and B–15 into equation B–16 and rearrangement finally leads to the following form of the XT3D flow expression, equation 31, between cells 1 and 2:

$$\begin{aligned} Q_{1,2} &= -Q_{2,1} \\ &= C_{1,2,(1,2)}\left(h_2-h_1\right) + C_{1,4,(1,2)}\left(h_4-h_1\right) + C_{1,5,(1,2)}\left(h_5-h_1\right) \\ &\quad + C_{1,6,(1,2)}\left(h_6-h_1\right) + C_{1,7,(1,2)}\left(h_7-h_1\right) \\ &\quad - C_{2,9,(1,2)}\left(h_9-h_2\right) - C_{2,10,(1,2)}\left(h_{10}-h_2\right) \\ &\quad - C_{2,11,(1,2)}\left(h_{11}-h_2\right) - C_{2,12,(1,2)}\left(h_{12}-h_2\right), \end{aligned} \tag{B–17}$$

where the conductance-like coefficients,

$$
\begin{aligned}
C_{1,2,(1,2)} &= \frac{\left(\frac{T_{xx_1}\Delta w_{1,2}}{L_{1,2}}\right)\left(\frac{T_{xx_2}\Delta w_{1,2}}{L_{2,1}}\right)}{\frac{T_{xx_1}\Delta w_{1,2}}{L_{1,2}}+\frac{T_{xx_2}\Delta w_{1,2}}{L_{2,1}}} \\
C_{1,4,(1,2)} &= \frac{\left(\frac{T_{xx_2}\Delta w_{1,2}}{L_{1,2}}\right)\left(\frac{T_{xy_1}\Delta w_{1,2}}{l_{1,4}}\right)\frac{D_{1,5}}{D_{1,4}+D_{1,5}}}{\frac{T_{xx_1}\Delta w_{1,2}}{L_{1,2}}+\frac{T_{xx_2}\Delta w_{1,2}}{L_{2,1}}} \\
C_{1,5,(1,2)} &= \frac{\left(\frac{T_{xx_2}\Delta w_{1,2}}{L_{1,2}}\right)\left(\frac{T_{xy_1}\Delta w_{1,2}}{l_{1,5}}\right)\frac{D_{1,4}}{D_{1,4}+D_{1,5}}}{\frac{T_{xx_1}\Delta w_{1,2}}{L_{1,2}}+\frac{T_{xx_2}\Delta w_{1,2}}{L_{2,1}}} \\
C_{1,9,(1,2)} &= \frac{\left(\frac{T_{xx_2}\Delta w_{1,2}}{L_{1,2}}\right)\left(\frac{T_{xz_1}\Delta w_{1,2}}{l_{1,9}}\right)\frac{D_{1,10}}{D_{1,9}+D_{1,10}}}{\frac{T_{xx_1}\Delta w_{1,2}}{L_{1,2}}+\frac{T_{xx_2}\Delta w_{1,2}}{L_{2,1}}} \\
C_{1,10,(1,2)} &= \frac{\left(\frac{T_{xx_2}\Delta w_{1,2}}{L_{1,2}}\right)\left(\frac{T_{xz_1}\Delta w_{1,2}}{l_{1,10}}\right)\frac{D_{1,9}}{D_{1,9}+D_{1,10}}}{\frac{T_{xx_1}\Delta w_{1,2}}{L_{1,2}}+\frac{T_{xx_2}\Delta w_{1,2}}{L_{2,1}}} \\
C_{2,9,(1,2)} &= \frac{\left(\frac{T_{xx_1}\Delta w_{1,2}}{L_{1,2}}\right)\left(\frac{T_{xy_2}\Delta w_{1,2}}{l_{2,9}}\right)\frac{D_{2,10}}{D_{2,9}+D_{2,10}}}{\frac{T_{xx_1}\Delta w_{1,2}}{L_{1,2}}+\frac{T_{xx_2}\Delta w_{1,2}}{L_{2,1}}} \\
C_{2,10,(1,2)} &= \frac{\left(\frac{T_{xx_1}\Delta w_{1,2}}{L_{1,2}}\right)\left(\frac{T_{xy_2}\Delta w_{1,2}}{l_{2,10}}\right)\frac{D_{2,9}}{D_{2,9}+D_{2,10}}}{\frac{T_{xx_1}\Delta w_{1,2}}{L_{1,2}}+\frac{T_{xx_2}\Delta w_{1,2}}{L_{2,1}}} \\
C_{2,11,(1,2)} &= \frac{\left(\frac{T_{xx_1}\Delta w_{1,2}}{L_{1,2}}\right)\left(\frac{T_{xz_2}\Delta w_{1,2}}{l_{2,11}}\right)\frac{D_{2,12}}{D_{2,11}+D_{2,12}}}{\frac{T_{xx_1}\Delta w_{1,2}}{L_{1,2}}+\frac{T_{xx_2}\Delta w_{1,2}}{L_{2,1}}} \\
C_{2,12,(1,2)} &= \frac{\left(\frac{T_{xx_1}\Delta w_{1,2}}{L_{1,2}}\right)\left(\frac{T_{xz_2}\Delta w_{1,2}}{l_{2,12}}\right)\frac{D_{2,11}}{D_{2,11}+D_{2,12}}}{\frac{T_{xx_1}\Delta w_{1,2}}{L_{1,2}}+\frac{T_{xx_2}\Delta w_{1,2}}{L_{2,1}}},
\end{aligned}
\tag{B–18}
$$

result from substitution of equation B–12 into equation 32, with transmissivities defined by

$$
\begin{aligned}
T_{xx_1} &= K_{xx_1}\left(A_{1,2}/\Delta w_{1,2}\right) \\
T_{xy_1} &= K_{xy_1}\left(A_{1,2}/\Delta w_{1,2}\right) \\
T_{xz_1} &= K_{xz_1}\left(A_{1,2}/\Delta w_{1,2}\right) \\
T_{xx_2} &= K_{xx_2}\left(A_{1,2}/\Delta w_{1,2}\right) \\
T_{xy_2} &= K_{xy_2}\left(A_{1,2}/\Delta w_{1,2}\right) \\
T_{xz_2} &= K_{xz_2}\left(A_{1,2}/\Delta w_{1,2}\right).
\end{aligned}
\tag{B–19}
$$

Note that $A_{1,2}/\Delta w_{1,2}$, the interfacial area divided by the interfacial width, is the interfacial thickness.

Coordinate-aligned anisotropy

When the principal directions of anisotropy are aligned with the x, y, and z coordinate axes, $K_{xy} = K_{xz} = 0$, and equations B–17 and B–18 reduce to

$$Q_{1,2} = -Q_{2,1} = C_{1,2,(1,2)} \left(h_2 - h_1\right) \tag{B–20}$$

with

$$C_{1,2,(1,2)} = \frac{\left(\frac{T_{xx_1}\Delta w_{1,2}}{L_{1,2}}\right)\left(\frac{T_{xx_2}\Delta w_{1,2}}{L_{2,1}}\right)}{\frac{T_{xx_1}\Delta w_{1,2}}{L_{1,2}} + \frac{T_{xx_2}\Delta w_{1,2}}{L_{2,1}}}. \tag{B–21}$$

The flow between cells 1 and 2 is then the product of the head difference between the cells and a conductance that is the harmonic mean of conductances calculated for cells 1 and 2.

Comparison with Straightforward Finite-Difference Discretization

To calculate the normal flux into cell 1 from cell 2 on the regular grid shown in figure B–1, a straighforward finite-difference discretization uses differencing along the primary connection to estimate the x component of the head gradient and along neighboring connections to estimate the y and z components of the head gradient (see, for example, discretization of the dispersion term in Zheng and Wang, 1999). For cell 1,

$$\begin{aligned}
\frac{\partial h}{\partial x} &\approx \frac{h_2 - h_1}{l_{1,2}} \\
\frac{\partial h}{\partial y} &\approx \frac{h_4 - h_5}{l_{1,4} + l_{1,5}} = \frac{(h_4 - h_1) + (h_1 - h_5)}{l_{1,4} + l_{1,5}} = \frac{l_{1,4}}{l_{1,4} + l_{1,5}}\left(\frac{h_4 - h_1}{l_{1,4}}\right) + \frac{l_{1,5}}{l_{1,4} + l_{1,5}}\left(\frac{h_1 - h_5}{l_{1,5}}\right) \\
\frac{\partial h}{\partial z} &\approx \frac{h_6 - h_7}{l_{1,6} + l_{1,7}} = \frac{(h_6 - h_1) + (h_1 - h_7)}{l_{1,6} + l_{1,7}} = \frac{l_{1,6}}{l_{1,6} + l_{1,7}}\left(\frac{h_6 - h_1}{l_{1,6}}\right) + \frac{l_{1,7}}{l_{1,6} + l_{1,7}}\left(\frac{h_1 - h_7}{l_{1,7}}\right).
\end{aligned} \tag{B–22}$$

Note that each of the central differences used to estimate the y and z components spans two connections, so each central difference can be expressed as the weighted average of finite differences across two connections, as shown in equation B–22. Substitution of equation B–22 into the x component of equation 7 (written in terms of the conductivity tensor for cell 1) then gives the following estimate of the normal flux into cell 1 from cell 2:

$$\begin{aligned}
q_{1,2} = \; & K_{xx_1}\left(\frac{h_2 - h_1}{l_{1,2}}\right) + K_{xy_1}\left[\frac{l_{1,4}}{l_{1,4} + l_{1,5}}\left(\frac{h_4 - h_1}{l_{1,4}}\right) + \frac{l_{1,5}}{l_{1,4} + l_{1,5}}\left(\frac{h_1 - h_5}{l_{1,5}}\right)\right] \\
& + K_{xz_1}\left[\frac{l_{1,7}}{l_{1,6} + l_{1,7}}\left(\frac{h_6 - h_1}{l_{1,6}}\right) + \frac{l_{1,6}}{l_{1,6} + l_{1,7}}\left(\frac{h_1 - h_7}{l_{1,7}}\right)\right].
\end{aligned} \tag{B–23}$$

Comparison of equation B–23—the flux expression derived by straightforward finite differencing—with equation B–13—the analogous flux expression calculated using the XT3D method—shows that the two flux expressions are similar in their general form on a rectangular grid:

- Each expression is the sum of "K_{xx}," "K_{xy}," and "K_{xz}" terms.
- In each expression, the K_{xx} term is based on an estimate of the x component of the head gradient obtained by differencing along the primary connection (the connection between cells 1 and 2).
- In each expression, the K_{xy} and K_{xz} terms are based on estimates of the y and z components of the head gradient obtained by taking weighted averages of finite differences along the connections oriented in the y and z directions, respectively.

Detailed comparison of the flow expressions also reveals the following differences on a rectangular grid:

- In the straightforward-finite-difference expression, the x component of the head gradient is obtained by differencing across the entire length of the primary connection. In the XT3D expression, the x component of the head gradient is obtained by differencing along the primary connection, but only between cell 1 and the primary interface. This difference is the result of an XT3D design decision to enforce continuity of flow at the primary interface by defining an interfacial head.
- In the straightforward-finite-difference expression, the distances used to calculate weights are connection lengths. In the XT3D expression, the distances used to calculate weights are distances from connection midpoints to the point where the primary connection intersects the primary interface. In XT3D, weights are based on a measure of the distance from the point at which gradient-component information is available (the midpoint of a connection) to the point at which the information is needed (a point on the primary interface). Instead of midpoint distances, connection lengths could have been chosen as an approximate measure.
- In the straightforward-finite-difference expression, the longer a connection, the more weight it receives in the gradient calculation. In the XT3D expression, the longer a connection, the farther its midpoint is from the intersection of the primary connection with the primary interface, and the less weight it receives in the gradient calculation.

Uniformly Spaced Grid

On a uniformly spaced grid with connection lengths l_x, l_y, and l_z along the x, y, and z directions, respectively, the straightforward-finite-difference flow expression, equation B–23, reduces to

$$q_{1,2} = K_{xx_1}\left(\frac{h_2 - h_1}{l_x}\right) + K_{xy_1}\left(\frac{h_4 - h_5}{2l_y}\right) + K_{xz_1}\left(\frac{h_6 - h_7}{2l_z}\right), \tag{B–24}$$

and the XT3D flow expression, equation B–13, reduces to

$$q_{1,2} = K_{xx_1}\left(\frac{h^*_{1,2} - h_1}{l_x}\right) + K_{xy_1}\left(\frac{h_4 - h_5}{2l_y}\right) + K_{xz_1}\left(\frac{h_6 - h_7}{2l_z}\right). \tag{B–25}$$

Publishing support provided by the U.S. Geological Survey
Science Publishing Network, Reston Publishing Service Center

For information concerning this publication, please contact:

Office of Groundwater
U.S. Geological Survey
Mail Stop 411
12201 Sunrise Valley Drive
Reston, VA 20192
(703) 648–5001
https://water.usgs.gov/ogw/

ISSN 2328-7055 (online)
https://doi.org/10.3133/tm6A56